Systems/Circuits

Somatic Integration of Incoherent Dendritic Inputs in the Gerbil Medial Superior Olive

Yarmo Mackenbach and J. Gerard G. Borst
Department of Neuroscience, Erasmus MC, University Medical Center Rotterdam, Rotterdam, 3000 CA, The Netherlands

The medial superior olive (MSO) is a binaural nucleus that is specialized in detecting the relative arrival times of sounds at both ears. Excitatory inputs to its neurons originating from either ear are segregated to different dendrites. To study the integration of synaptic inputs both within and between dendrites, we made juxtacellular and whole-cell recordings from the MSO in anesthetized female gerbils, while presenting a "double zwuis" stimulus, in which each ear received its own set of tones, which were chosen in a way that all second-order distortion products (DP2s) could be uniquely identified. MSO neurons phase-locked to multiple tones within the multitone stimulus, and vector strength, a measure for spike phase-locking, generally depended linearly on the size of the average subthreshold response to a tone. Subthreshold responses to tones in one ear depended little on the presence of sound in the other ear, suggesting that inputs from different ears sum linearly without a substantial role for somatic inhibition. The "double zwuis" stimulus also evoked response components in the MSO neuron that were phase-locked to DP2s. Bidendritic subthreshold DP2s were quite rare compared with bidendritic suprathreshold DP2s. We observed that in a small subset of cells, the ability to trigger spikes differed substantially between both ears, which might be explained by a dendritic axonal origin. Some neurons that were driven monaurally by only one of the two ears nevertheless showed decent binaural tuning. We conclude that MSO neurons are remarkably good in finding binaural coincidences even among uncorrelated inputs.

Key words: **binaural coincidences; distortion products; excitatory inputs; phase-locking; sound localization; vector strength**

Significance Statement

Neurons in the medial superior olive are essential for precisely localizing low-frequency sounds in the horizontal plane. From their soma, only two dendrites emerge, which are innervated by inputs originating from different ears. Using a new sound stimulus, we studied the integration of inputs both within and between these dendrites in unprecedented detail. We found evidence that inputs from different dendrites add linearly at the soma, but that small increases in somatic potentials could lead to large increases in the probability of generating a spike. This basic scheme allowed the MSO neurons to detect the relative arrival time of inputs at both dendrites remarkably efficient, although the relative size of these inputs could differ considerably.

Introduction

To localize low-frequency sounds, we rely heavily on a nucleus located in the brainstem called the medial superior olive (MSO), which compares the arrival times of excitatory signals from both cochlear nuclei. MSO principal neurons act as coincidence detectors (Goldberg and Brown, 1969; Moushegian et al., 1975; Langford, 1984; Yin and Chan, 1990; Spitzer and Semple, 1995; van der Heijden et al., 2013), as they preferentially fire when inputs from both ears arrive simultaneously. This happens at the "best" interaural time difference (BITD), at which point a difference in sound arrival times compensates for the difference in internal travel time from either ear.

Its principal neurons have a relatively simple morphology and wiring. They have a spindle-shaped soma and typically two primary dendrites (Goldberg and Brown, 1968; Smith, 1995; Rautenberg et al., 2009). The medial and lateral dendrite receive inputs from spherical bushy cells of the contralateral and the ipsilateral cochlear nucleus, respectively; in addition, these neurons receive somatic inhibitory inputs from the ipsilateral medial nucleus of the trapezoid body (MNTB) and the contralateral lateral nucleus of the trapezoid body (Thompson and Schofield,

Received Nov. 30, 2022; revised Apr. 11, 2023; accepted Apr. 14, 2023.

Author contributions: Y.M. and J.G.G.B. designed research; Y.M. performed research; Y.M. and J.G.G.B. analyzed data; Y.M. and J.G.G.B. wrote the paper.

This work was supported by NWO (ALW-open, Great Timing, #824.15.008). We thank Marcel van der Heijden for designing and implementing the binaural zwuis method and analysis; and Martijn Sierksma for commenting on an earlier version of this manuscript.

The authors declare no competing financial interests.

Correspondence should be addressed to J. Gerard G. Borst at g.borst@erasmusmc.nl.

https://doi.org/10.1523/JNEUROSCI.2215-22.2023

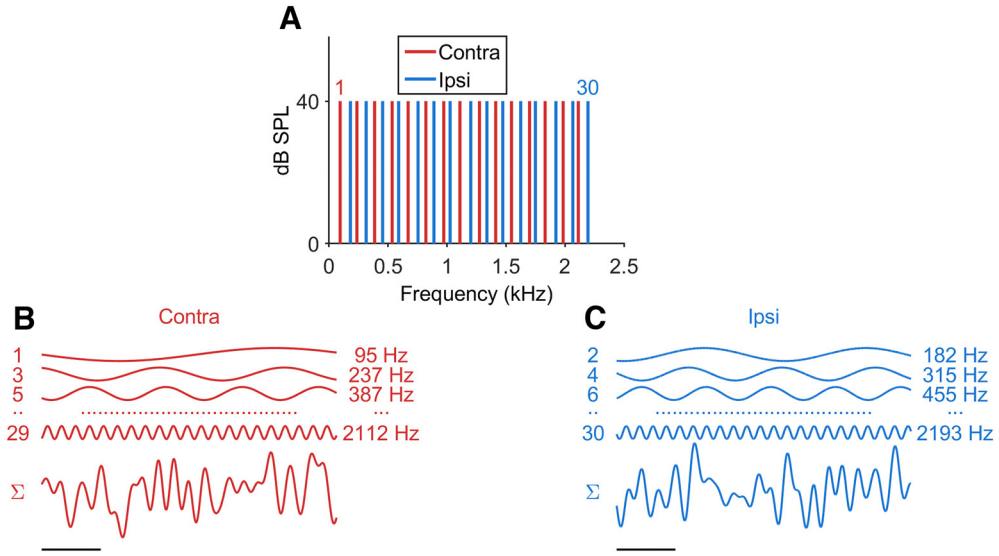

Figure 1. DZW stimulus. ***A***, The DZW stimulus consisted of a total of 30 frequency components, which were distributed across ipsilateral (blue) and contralateral (red) ears. Its usage was combined with the complementary stimulus, in which the frequency components were swapped across the ears (not shown). In the monaural versions of this stimulus, either the contralateral or the ipsilateral components were left out. ***B***, The zwuis stimulus played in this presentation to the contralateral ear consisted of a combination of pure tones, of which 10 ms of the first three (1, 3, 5) and the last (29) is shown. The (rounded) frequency (in Hz) of these four sine waves is given to the right of the traces. Bottom row represents the sum (Σ) of all 15 components. ***C***, Same as in ***B***, but illustrating the even components (2, 4, 6,..., 30) of the DZW stimulus, which, in this presentation, were played concurrently (Σ trace) to the ipsilateral ear.

2000). Action potentials (APs) are initiated within the axon (Scott et al., 2007), which typically originates from the soma in gerbils (Kuwabara and Zook, 1999; Scott et al., 2005; Rautenberg et al., 2009).

Because of the segregation of the inputs from both ears to different dendrites, the MSO neurons are highly suitable to study the integration of different inputs *in vivo* both within a dendrite and between dendrites. Our previous experiments provided evidence that the somatic summation of inputs from both dendrites is a linear process, but that spike initiation shows an expansive nonlinear dependence on the EPSP amplitude (van der Heijden et al., 2013). This mechanism enables MSO neurons to act as a coincidence detector and provides a cellular explanation for binaural facilitation, which is the observation that the firing rate of MSO neurons for binaural stimulation at the BITD is typically higher than the sum of the rates evoked by monaural stimuli (Goldberg and Brown, 1969; Yin and Chan, 1990; Spitzer and Semple, 1995). We obtained further evidence for linear somatic summation of dendritic inputs by comparing the monaural and the binaural response to a wideband tone complex stimulus ("zwuis"). The relationship between the firing rate and the ITD could be well predicted from the subthreshold monaural responses, in agreement with the idea that MSO neurons function as simple cross-correlators of their bilateral inputs (Plauška et al., 2016). In contrast, other studies have found evidence that the inputs from both ears interact nonlinearly, both *in vivo* (Brand et al., 2002; Pecka et al., 2008; Franken et al., 2015) and in slices (Grothe and Sanes, 1994; Myoga et al., 2014).

ITD tuning has often been assessed using binaural beats, in which two tones with slightly different frequencies are played to the left and right ear (Yin and Chan, 1990; Spitzer and Semple, 1995; Batra et al., 1997; van der Heijden et al., 2013). This stimulus has the advantage that the phase difference between the stimuli from both ears is continuously changing, allowing to study the relation between, for example, firing rate and ITD at high resolution. However, synaptic integration both across and within one ear is limited since it is not a wideband stimulus. Our aim is to study the synaptic integration both across and within dendrites along the frequency range relevant for MSO neurons, and to study the relative efficacy at which these different interactions result in APs. To study the postsynaptic integration of inputs more systematically, we used a new stimulus, which we call "double zwuis" (DZW). With DZW, each ear receives its own irregular tone complex stimulus (see Fig. 1). The tone frequencies are chosen such that not only all tones are unique, but that each sum or difference frequency (second-order distortion product [DP2]) both between and within ears is unique as well. This stimulus is thus a generalization of binaural beats, which have previously been used to analyze MSO responses (Yin and Chan, 1990; van der Heijden et al., 2013; Franken et al., 2015), with the advantage of generating hundreds of different interactions both between and within ears that are uniquely identifiable. We applied this stimulus in gerbils, since they have good low-frequency hearing (Ryan, 1976) and can localize low-frequency sounds relatively well (Maier and Klump, 2006). The DZW stimulus allowed us to study in unprecedented detail how inputs interact and how this generates APs in the MSO.

Materials and Methods

Animal procedures

All experiments were conducted in accordance with the European Communities Council Directive (86/609/EEC) and approved by the institutional animal ethics committee.

Young-adult female Mongolian gerbils (88 ± 22 d postnatal; range 51-141 d; $n = 39$) with an average body weight of 62.5 ± 5.3 g (range 54-76 g) were anesthetized intraperitoneally with a 0.01 ml/g body weight injection of ketamine-xylazine solution (1% and 0.15%, respectively) to give a concentration of 100 mg/kg ketamine and 15 mg/kg xylazine. Reflexive state was monitored throughout the experiment by performing the hindpaw pinch-reflex test and was maintained by regular administration of the same ketamine-xylazine solution. Body core temperature was monitored using a rectal probe, and maintained at 37°C using an adjustable electrical heating pad.

The head was fixed using a metal head plate that was glued to an exposed rostrodorsal part of the skull. Both pinnae were removed, providing access to the ear canal for placing the tubes for delivering sound stimuli. The animal was fixed in a supine position. The skin, connective

tissue, salivary glands, and lymph nodes above the trachea were surgically removed, followed by a tracheotomy and intubation, after which the animal kept breathing independently. Both bullae were exposed by removing the overlying muscles and making openings in the bone using a scalpel and forceps. The opening of both bullae equalizes the effect of opening on low-frequency middle ear transfer (Ravicz et al., 1992). A 0.3-mm-diameter craniotomy was made on the right side using a drill. The craniotomy was located ~2 mm rostrally from the stapedial artery and in the middle between the cochlea and the medial wall of the skull. When needed, the craniotomy was extended by drilling. The angle of the electrode insertion point could be changed with the use of a fixed-pivotal-point, custom-built positioning device on which the animal rested throughout the experiment.

In vivo *electrophysiology*

Recordings were made with thick-walled borosilicate glass microelectrodes having a resistance of 4-7 MΩ when filled with recording solution. Pipettes were filled with a solution that contained the following (in mM): 138 K-gluconate, 8 KCl, 10 Na_2-phosphocreatine, 4 MgATP, 0.3 Na_2GTP, 0.5 EGTA, and 10 mM HEPES (pH 7.2 with KOH). In a minority of the cells (<10%), recordings were made using extracellular solution, which contained the following (in mM): 135 NaCl, 5.4 KCl, 1 $MgCl_2$, 1.8 $CaCl_2$, and 5 mM HEPES (pH 7.2 with NaOH). No specific differences could be found between the responses of cells recorded with either solution, so we pooled them for the analysis. High positive pressure (~100 mbar) was applied to the pipettes during brain surface penetration. Immediately after successful penetration of the brain surface, the pressure was lowered to 20-30 mbar, and we waited for a few minutes before making a recording to minimize the impact of brain tissue movements relative to the electrode. The location of the MSO somatic layer was identified on the basis of the local field potential ("neurophonics") (Galambos et al., 1959; Biedenbach and Freeman, 1964; Clark and Dunlop, 1968; McLaughlin et al., 2010; Goldwyn et al., 2017), as described previously (van der Heijden et al., 2013). Field potentials were evoked using monaural click stimuli (2 ms duration) presented alternately to either ear. Once the somatic layer was reached, the pipette was advanced slowly and its resistance was monitored closely. Contacting a neuron resulted in a gradual increase in resistance, after whch we released positive pressure. For whole-cell recordings, suction was applied to obtain the cell-attached configuration; the whole-cell configuration was established by suction pulses, which was apparent as a negative jump in the recorded potential; whole-cell recordings were compensated for an estimated junction potential of −11 mV. In the case of juxtacellular (loose-patch) recordings, no suction was applied; typically, the resistance reached a value of 20-40 MΩ. All recordings were done in current-clamp mode, while the seal resistance was regularly monitored. In response to small changes in seal resistance, the bridge balance and capacitance compensation were readjusted in between sets of recordings. In case of evident changes in cell responses, the recordings were stopped. Data were acquired using a MultiClamp 700B amplifier (Molecular Devices) with custom software written in MATLAB (The MathWorks).

Auditory stimulation

Auditory stimuli were generated using custom MATLAB software and realized through a 24-bit digital-to analog channel processor [RX6; Tucker Davis Technologies (TDT); 111.6 kHz], programmable attenuator (PA5; TDT), and an amplifier (SA1; TDT). Stimuli were presented in a close-field configuration to the animal with Shure speakers (frequency range 22 Hz to 17.5 kHz) attached to the ear canal via a small tube (length ~11 cm). The correct stimulus levels and phases were attained by calibrating the drivers in situ at the level of the tympanic membrane using a microphone housed in the probe. The transfer characteristics of the probe were taken into account.

For this study, we used a new DZW multitone stimulus (see Fig. 1) derived from the previously described zwuis stimulus (van der Heijden and Joris, 2003). Irregularly spaced tones were segregated across both ears to generate a stimulus that had similar tonal characteristics for both ears, yet had no binaural correlation. None of the frequencies of the principal components overlapped with each other or the second- and third-order distortion products. The principal components ranged from ~100 Hz to 2200 Hz (mean spacing: 72 Hz; see Fig. 1*A*). The stimulus was presented for ~48 s (including 1 s prestimulus and poststimulus baselines) and consisted of two types of presentations: the odd components presented to the left (contralateral) ear and even to the right (ipsilateral) ear (see Fig. 1), or the opposite tonal distribution. The order of these two presentations was randomized for each cell. The stimulus could be presented monaurally or binaurally, resulting in a succession of three presentations (each with the two presentations), which we will refer to as a DZW triplet; the order of these three presentations was also randomized for each cell. To approximate overall sound pressure levels used before in our MSO experiments with different auditory stimuli, the DZW was presented at 40 dB SPL per component (see Fig. 1*A*). If the recordings were stable enough, the stimulus was also presented at different sound intensities. All components had the same amplitude and a random phase (van der Heijden and Joris, 2006; Versteegh and van der Heijden, 2012).

Additional auditory stimuli were presented whenever the recording quality permitted this. The DZW stimulus was also presented at an intensity of 30 dB per component, which should reduce crosstalk between the two ears. To determine frequency tuning to tones we presented randomized pure tones ranging from 0.1 to 30 kHz, 70 ms each; these tones were presented at sound intensities ranging from 10-40 dB SPL. To determine the BITD of a cell, we presented Gaussian noise binaurally [50 to 8000 Hz bandwidth, 300 ms burst for each condition, 21 different ITD values (conditions), and 20 repetitions; total duration of stimulus: 86 s].

Admission/selection criteria

Admission criteria based on recording quality. Loose-patch (juxtacellular) recordings were previously shown to be suitable to resolve synaptic events in MSO neurons (van der Heijden et al., 2013). We observed that the best quality loose-patch recordings were made when the seal resistance was between 20 and 70 MΩ; at lower resistances, the contamination with field potentials became too high, whereas higher resistances caused strong waveform filtering. In this study, only recordings with seal resistances between 20 and 70 MΩ were therefore accepted for analysis. Cells were also only accepted when they were located inside the somatic layer, confirmed by the double reversal of field potentials (see "neurophonics" above).

Post hoc *admission criteria.* Each new stimulus block was preceded by a silent period of 1 s. These baseline periods were used to judge recording stability. Details of the method were presented by Plauška et al. (2016). Briefly, a power spectrum of prestimulus and poststimulus baselines was estimated for all recordings from a cell. Its value at 1 kHz predominantly reflected the spontaneous inputs of the neuron. For a recording to be considered stable, the difference between prestimulus and poststimulus values had to remain within 2 dB. Between all recordings in a "DZW triplet" (two monaural + one binaural presentations, all at the same sound intensity), the difference between each value at 1 kHz (mean of prestimulus and poststimulus values) was not allowed to exceed 2 dB.

Data analysis

Event detection. APs of MSO neurons are strongly attenuated during back propagation (Scott et al., 2007). Despite their small amplitude in juxtacellular recordings, they can still be discriminated from subthreshold events by their faster repolarization rate (van der Heijden et al., 2013). APs were detected offline based on a manually set threshold criterion for the maximum repolarization rate of individual events (van der Heijden et al., 2013). Only cells for which histograms of negative peak sizes showed clear bimodality were accepted for further analysis.

Vector strength (VS). VS (Goldberg and Brown, 1969) was obtained by applying a Fourier transform to the binary event signal denoting the timing of the spikes and normalizing this to the number of spikes (Johnson, 1974).

Waveform processing. In analyses requiring cycle periodograms, waveforms were detrended with a 5 Hz high pass filter (using a truncated

Fourier transform). In analyses focusing on EPSP data, spikes were truncated by linearly interpolating the regions surrounding the detected APs (from 1 ms before to 1.2 ms after the peak of the spike).

BITD. BITD was determined using noise stimuli presented at different ITDs as described previously (Plauška et al., 2017). Positive ITDs correspond to the signal leading at the contralateral ear.

Baseline power compensation. Because of the stereotypical time course of elementary subthreshold events, they contribute to the power spectrum of the cell's response to the DZW stimulus. An estimate for this spectral contamination can be obtained from the power spectrum of the baseline (Plauška et al., 2017), which was estimated by calculating power spectral densities using Welch's method. The power spectral density values of the different baselines of each DZW triplet were pooled and fitted using a polynomial fit. This power spectral density fit was then used to correct the magnitudes of Fourier transforms performed on any of the recordings belonging to the DZW triplet; frequencies <100 Hz were left uncorrected.

Estimating power of subthreshold and suprathreshold components in DZW response. The total power of primary, monodendritic DP2 or bidendritic DP2 subthreshold responses was obtained by converting the magnitudes (in dB), obtained by Fourier analysis, of the relevant, significant subthreshold components in response to binaural DZW stimulation to power and summing them. An estimate for the total power of suprathreshold components was obtained from the sum of the squared VS values for significant components. To display ratios of non-zero powers, they were converted to a dB scale.

Spontaneous spike rate compensation. The spontaneous spike rate was computed by averaging the spike rates during the baselines of a DZW triplet. Spike rates during monaural stimulation were corrected for the spontaneous spike rate using the following rules. If the measured spike rate was equal to the spontaneous spike rate, the stimulus apparently did not have any effect (corrected spike rate = measured spike rate – spontaneous spike rate). If the measured spike rate was at least twice the spontaneous spike rate, it was assumed that the stimulated side no longer generated spontaneous spikes while the nonstimulated ear still did; therefore, only half the spontaneous spike rate was used for correction (corrected spike rate = measured spike rate – spontaneous spike rate $\times$ 0.5). If the evoked rate was in between the two previous scenarios, the portion of spontaneous spike rate used to correct was linearly proportional to the ratio of spontaneous spike rate/measured spike rate (corrected spike rate = measured spike rate – spontaneous spike rate $\times$ spontaneous spike rate/measured spike rate). Spike rates for binaural stimulations were not adjusted, as we assumed that spontaneous inputs no longer contributed to spike generation under these conditions (van der Heijden et al., 2013).

How well do MSO neurons function as coincidence detectors?. The measurement of VSs during monaural and binaural DZW allowed us to compare the performance of MSO cells with an ideal coincidence detector. In an ideal coincidence detector, the VS of individual components will not be smaller during binaural stimulation. In this section, we define the metric θ for the performance of a coincidence detector by also evaluating the opposite case, in which there is no coincidence detection at all. The binaurally evoked spike trains can then be described as a simple superposition of two monaurally evoked spike trains. In this analysis, we neglect the role that spontaneous inputs from the nonstimulated dendrite may play in spike generation during monaural stimulation (Colburn et al., 1990; van der Heijden et al., 2013). From the definition of VS as the first Fourier component normalized by spike count, binaural spike-train superposition would lead to the following simple predicted relation between monaurally evoked VSs S_M and binaurally evoked VS S_B as follows:

$$N_M S_M = N_B S_B \ (\text{assuming spike} - \text{train superposition}) \tag{1}$$

where the spike counts are denoted by N_M and N_B, and the subscript M (monaural) stands for either I (ipsilateral) or C (contralateral). The relation holds separately for each frequency component. The assumption of simple spike train superposition that led to Equation 1, however, also predicts that the binaural spike count is the sum of the monaural spike counts (i.e., $N_B = N_C + N_I$). What is missing from Equation 1 is the possibility of tonic effects of binaural stimulation, that is, effects of stimulating the other ear that affect spike rate, but not spike timing. In order to eliminate such tonic effects from the analysis of spike timing, the binaural spike rate of Equation 1 must be corrected by a factor $(N_C + N_I)/N_B$, leading to the following:

$$N_M S_M = (N_C + N_I) S_B \ (\text{assuming no coincidence detection}) \tag{2}$$

This expresses an expectation of the relation between monaural and binaural VS in the hypothetical case that spikes are phase-locked to the inputs from either ear, but not to both at the same time. Thus, when comparing monaural stimulation to binaural stimulation, the introduction of the (interaurally uncorrelated) stimulus to the other ear is predicted to reduce all VSs by a factor of $N_M/(N_C + N_I)$ as follows:

$$\beta_C \triangleq \frac{S_B}{S_C} = \frac{N_C}{N_C + N_I},$$

$$\beta_I \triangleq \frac{S_B}{S_I} = \frac{N_I}{N_C + N_I} (\text{assuming no coincidence detection}) \tag{3}$$

This is the prediction of the baseline case of spike-train superposition, in which the spikes can phase-lock to either ear but not to both at the same time. Thus, we observed a systematic reduction of phase-locking caused by stimulating the opposite ear (i.e., the MSO cell is not a perfect coincidence detector), but the reduction is less severe than is expressed in Equation 3. Clearly, the phase-locking of the actual MSO cell is more robust against stimulating the other ear than predicted for the simple spike-train superposition, in agreement with its well-known operation as a coincidence detector. If the monaurally evoked spike trains would simply add, so would their Fourier spectra, and binaural beat responses would not show phase-locking to the beat frequency. This prediction is strongly violated by binaural beat data (Yin and Chan, 1990; Spitzer and Semple, 1995; van der Heijden et al., 2013). The other extreme, a perfect coincidence detector, has all spikes optimally phase-locked to both ears, and the introduction of the stimulus to the other ear would have no effect on phase-locking, i.e., $S_B = S_M$ and $\beta_{C,I} = 1$.

As a metric for where the actual data lie relative to these two extremes, we define the metric θ by normalizing the fitted slope β to the baseline value of spike-train superposition as follows:

$$\begin{aligned} \theta_C &= \left(1 + \frac{N_C}{N_I}\right)\beta_C - \frac{N_C}{N_I} \\ \theta_I &= \left(1 + \frac{N_I}{N_C}\right)\beta_I - \frac{N_I}{N_C} \end{aligned} \tag{4}$$

θ_C and θ_I quantify to what extent the MSO neuron is an ideal coincidence detector. Specifically, θ_C describes how robust phase-locking to the contralateral stimulus is against stimulating the ipsilateral ear, and θ_I captures the reverse case. $\theta = 0$ corresponds to minimal robustness as predicted by a total lack of coincidence detection (Eq. 3). $\theta = 1$ corresponds to the ideal coincidence detector for which VS in one ear is unaffected by stimulating the opposite ear.

Spike triggering efficacy. Spike triggering efficacy was defined as the slope of the fit through the origin of the relation between significant VS and subthreshold components for a certain type of stimulus (e.g., contralateral + primary + binaural). A minimum of three data points was required for fitting.

Software

All data processing and analysis were performed using custom software written in MATLAB.

Experimental design and statistical analysis

The experimental design is described above under Auditory stimulation. Statistical significance of principal components and DP2s

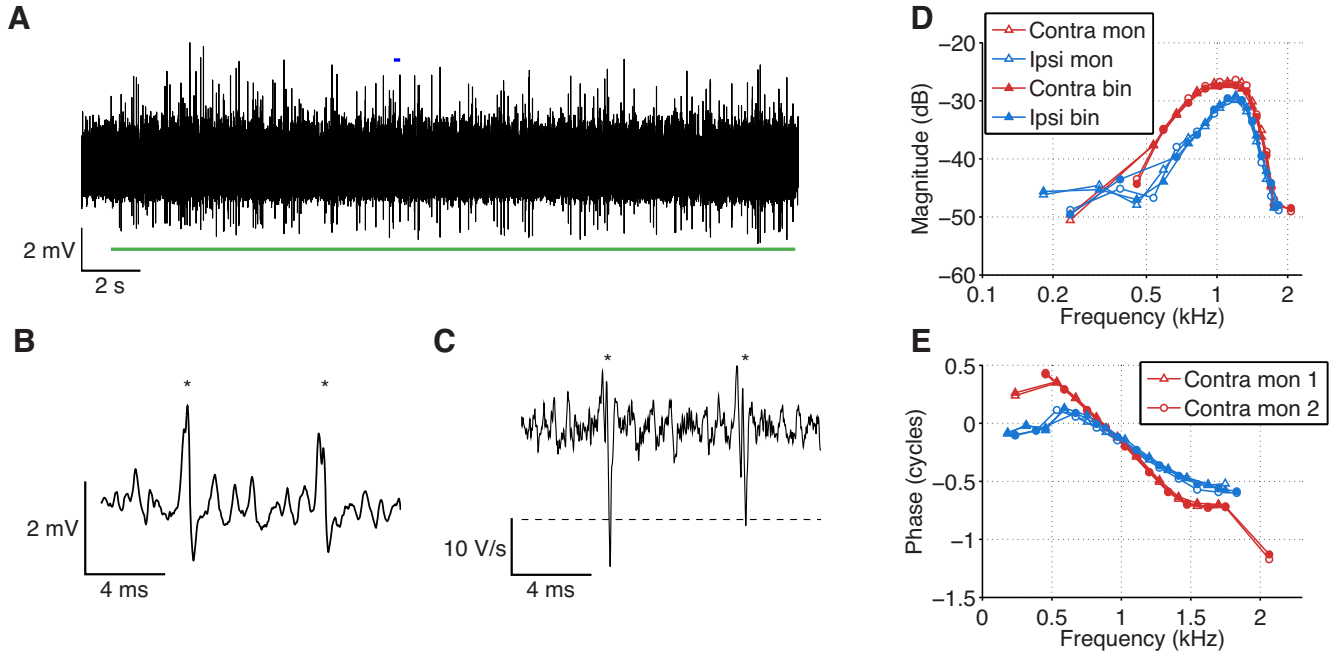

Figure 2. Response to the DZW stimulus and analysis of subthreshold responses. ***A***, Example of the response of an MSO cell (86604) to the DZW stimulus during a juxtacellular recording. Green bar represents auditory stimulation. ***B***, Short segment of the recording extracted from underneath the blue square shown in ***A*** showing two sound-evoked APs marked by *. ***C***, First derivative of the recording shown in ***B***. Broken line indicates criterion for AP. The two APs are again marked by *. ***D***, Frequency responses to 40 dB SPL DZW stimulation, as estimated from the Fourier spectrum of the response waveform (the high-pass filtered recorded potential) restricted to subthreshold activity (i.e., after the removal of the APs). Subthreshold response magnitudes were similar for binaural (filled symbols) and monaural (empty symbols) stimulation. In both cases, frequency components of the same presentation are connected, and each frequency is presented to both ears in consecutive presentations, referred to as Presentation 1 (triangles) and Presentation 2 (circles), respectively. Only components passing the Rayleigh test (see Materials and Methods) are shown here. In this and following figures, 0 dB corresponds to an amplitude of 1 mV. ***E***, Corresponding phases of the subthreshold responses. Symbols have the same meaning as in ***D***. Phases have been compensated for a delay of 4.3 ms. Same cell as shown in ***A***-***D***.

was determined by a Rayleigh test ($p < 0.0001$) applied to the phase values obtained by segmenting the response waveform into 10 equally long, nonoverlapping segments (Versteegh and van der Heijden, 2012). Other statistical tests are described in the text. Results are presented as mean ± SD.

Results

DZW stimulus

To systematically investigate how principal neurons of the MSO integrate inputs originating from both ears, we used a binaural multitone stimulus called DZW. It is a binaural version of the multitone zwuis stimulus previously applied to auditory nerve responses (van der Heijden and Joris, 2003), otoacoustic emissions (Meenderink and van der Heijden, 2011), cochlear-mechanical measurements (Versteegh and van der Heijden, 2012), and MSO neurons (Plauška et al., 2016). The difference with earlier incarnations is that DZW is a binaural form of zwuis, whose frequency components are presented alternately to either ear (Fig. 1). Each recording was followed by one in which the frequencies were interchanged between the ears. This distribution of frequency components provides a way to apply binaural stimulation and obtain a response whose primary spectral components can be traced back with certainty to either the ipsilateral or contralateral ear. Unlike previous studies, in which an identical zwuis stimulus was successively presented to each of the two ears (Plauška et al., 2016), the new stimulus also allows a direct analysis of the interaction between the primaries in the form of distortion products (DP2s). Here we used this rich stimulus to investigate how different inputs to the MSO neurons interact to trigger spikes. We will first describe the responses to the subthreshold and the suprathreshold primaries and their relation, followed by the subthreshold and suprathreshold DP2s and their relation.

Difference between monaural and binaural subthreshold responses

Subthreshold responses

We made juxtacellular ($n = 65$) and whole-cell recordings ($n = 6$) from principal neurons of the MSO while presenting the DZW stimulus to the gerbils (Fig. 2*A*,*B*). In juxtacellular MSO cell recordings, APs (marked with * in Fig. 2*B*) generally have a similar amplitude as the EPSPs that generated them, but they can be discriminated on the basis of the repolarization rate, which is faster for APs than for EPSPs (Fig. 2*C*) (van der Heijden et al., 2013). Fourier analysis of the subthreshold responses shows the frequency tuning of the ipsilateral and contralateral inputs (Fig. 2*D*) and the corresponding phase curves (Fig. 2*E*). The frequencies that were presented to the ipsilateral ear were subsequently presented to the contralateral ear and vice versa. In this way, each frequency component of the zwuis stimulus is represented in both the ipsilateral and contralateral analysis. The data in Figure 2*D* combine these two presentations. In addition, DZW stimuli were presented not only binaurally but also monaurally, by omitting the 15 frequency components presented to one of the ears. The monaural data are shown as open symbols in Figure 2*D*; the binaural data are represented by the closed symbols.

The comparison of the binaural and monaural responses allowed us to assess to what extent the presence of inputs from one ear affected the size and timing of the subthreshold responses to the inputs from the other ear. In the cell shown in Figure 2, the magnitude and phase of the subthreshold responses were remarkably little affected by the presence or absence of

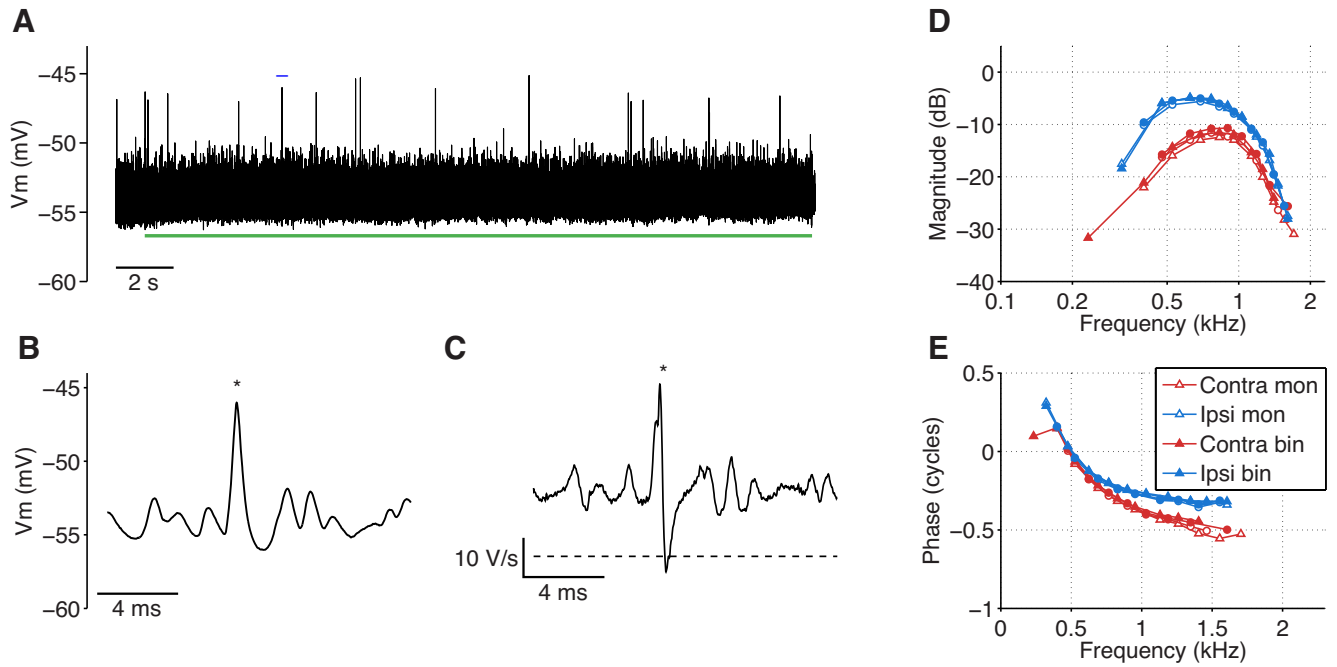

Figure 3. Whole-cell recordings showed similar results as juxtacellular recordings. ***A***, Example of the response to the DZW stimulus of an MSO cell (86108) recorded in the whole-cell configuration. Green bar represents auditory stimulation. ***B***, Short segment of the recording extracted from underneath the blue square shown in ***A***. *Single spike. ***C***, First derivative of the recording segment shown in ***B***. *Single spike. Broken horizontal line indicates the AP criterion. ***D***, Frequency responses to 40 dB SPL DZW stimulation, as estimated from the Fourier spectrum of the response waveform of the same cell as shown in ***A-C***. Response magnitudes were similar for binaural (filled symbols) and monaural (empty symbols) stimulation. In both cases, frequency components of the same presentation are connected, and each frequency is presented to both ears in consecutive presentations, referred to as Presentation 1 (triangles) and Presentation 2 (circles), respectively. ***E***, Phases of the phase-locked responses to the different frequencies in the DZW stimulation. Symbols have the same meaning as in ***D***. Phases have been compensated for a delay of 5.2 ms.

sound stimulation at the other ear (compare closed and open symbols in Fig. 2*D*).

Since the amplitude of events measured in juxtacellular recordings depends on the local membrane resistance, we checked whether the similarity in the responses to monaural and binaural stimulation was also observed in whole-cell recordings in 6 cells. An example whole-cell recording showing the response to the DZW stimulus is shown in Figure 3. Similar to juxtacellular recordings, magnitude and phase of subthreshold responses differed little in response to monaural and binaural stimulation (Fig. 3*D*,*E*). Our data suggest that juxtacellular recordings are a reliable alternative for whole-cell recordings for quantitative analysis of subthreshold activity in MSO cells, in agreement with our previous results (van der Heijden et al., 2013). This is important as both the success rate and stability of juxtacellular recordings were higher than for whole-cell recordings.

The difference between monaural and binaural responses of the cell shown in Figure 2*D* is analyzed in Figure 4*A*, *B*. The magnitude difference amounted to maximally 2.3 dB (~30%). The maximum phase shift was 0.04 cycles, corresponding to 0.02 ms at 2065 Hz. A comparison of the response to monaural and binaural stimuli in a population of cells ($n = 71$, juxtacellular recordings and whole-cell recordings pooled together) showed that magnitude (Fig. 4*C*) and phases (Fig. 4*D*) of the subthreshold responses were generally similar. On average, the maximum difference in the magnitude was <1 dB for all frequency bins and the average phase shift was <0.1 cycle across all frequencies. The variability was generally higher for ipsilateral than for contralateral responses. Similar results were obtained when responses were averaged relative to the best frequency of each cell (Fig. 4*E*,*F*).

Closer inspection of the different cells showed that a small number of cells did show a substantial change in the magnitude of the response between monaural and binaural stimuli at 40 dB SPL. Changes in both directions were observed. One example is shown in Figure 5*A*, for which the response to the ipsilaterally presented frequencies was clearly smaller for the monaural than for the binaural zwuis version, without a phase difference (Fig. 5*B*). In the same cell, the DZW stimulus was also presented at 30 dB SPL. At this intensity, the difference in the response to monaural and binaural DZW was strongly reduced (Fig. 5*C*), still without phase differences (Fig. 5*D*). Figure 5*E* illustrates that differences were always smaller at 30 dB SPL for the subset of cells ($n = 16$) that were tested at both 30 and 40 dB SPL. Figure 5*E* also contains one cell marked by diamond symbols that was recorded in the whole-cell recording configuration, which gave similar results as the cells with juxtacellular recordings.

Overall, the findings shown in Figures 2-5 show that the subthreshold response evoked by stimulating one ear is hardly affected by simultaneously stimulating the other ear. We therefore conclude that, to a good approximation, the two subthreshold responses evoked by wideband stimuli sum linearly across the ears, in agreement with previous studies that used simple tonal stimuli (Kuokkanen et al., 2013; van der Heijden et al., 2013; Plauška et al., 2016; Lu et al., 2018). A more accurate test of linearity, based on the analysis of distortion products in the response, will be presented further on.

APs

We next analyzed the APs evoked by the DZW stimuli. MSO neurons are generally not well driven by monaural stimuli (Goldberg and Brown, 1969; Yin and Chan, 1990; Spitzer and Semple, 1995), but we obtained sufficient data in a subset of cells to compare spike rates in response to monaural ipsilateral and contralateral DZW stimuli (Fig. 6*A*). A few cells were dominated

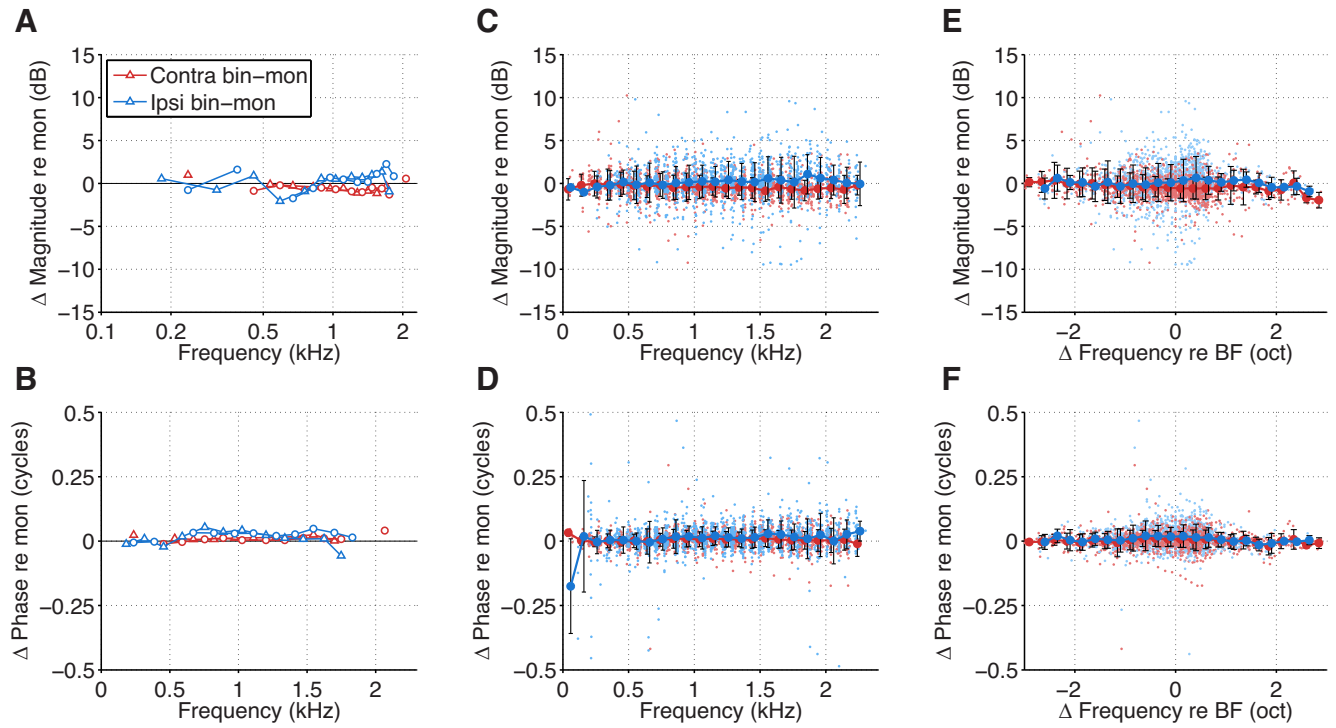

Figure 4. Comparison of subthreshold responses elicited by binaural and monaural DZW stimuli. ***A***, Difference in magnitude of responses to binaural and monaural DZW stimulation of the cell shown in Figure 1. Positive values signify larger amplitudes for binaural stimulation. ***B***, Companion phase differences. ***C***, Difference in the magnitude of the response to monaural and binaural DZW stimulation for a population of cells. Juxtacellular recordings ($n = 65$) and whole-cell recordings ($n = 6$) were pooled as results were similar for both methods. Each dot represents the difference in the response to a single primary component in a cell during binaural versus monaural DZW stimulation; for positive values, the binaural response was larger than the monaural response. Closed circles represent the averages of all responses in 100 Hz bins; for display purposes, the contralateral average responses have been slightly shifted in ***A*** and ***B***. ***D***, Same as in ***C***, but the phase of the response to monaural and binaural DZW stimulation was compared. Positive values correspond to a phase lead of the binaural response. ***E***, Same as in ***C***, but the stimulus frequencies are shown relative to the best frequency of each cell. ***F***, Same as in ***D***, but frequencies were normalized as in ***E***.

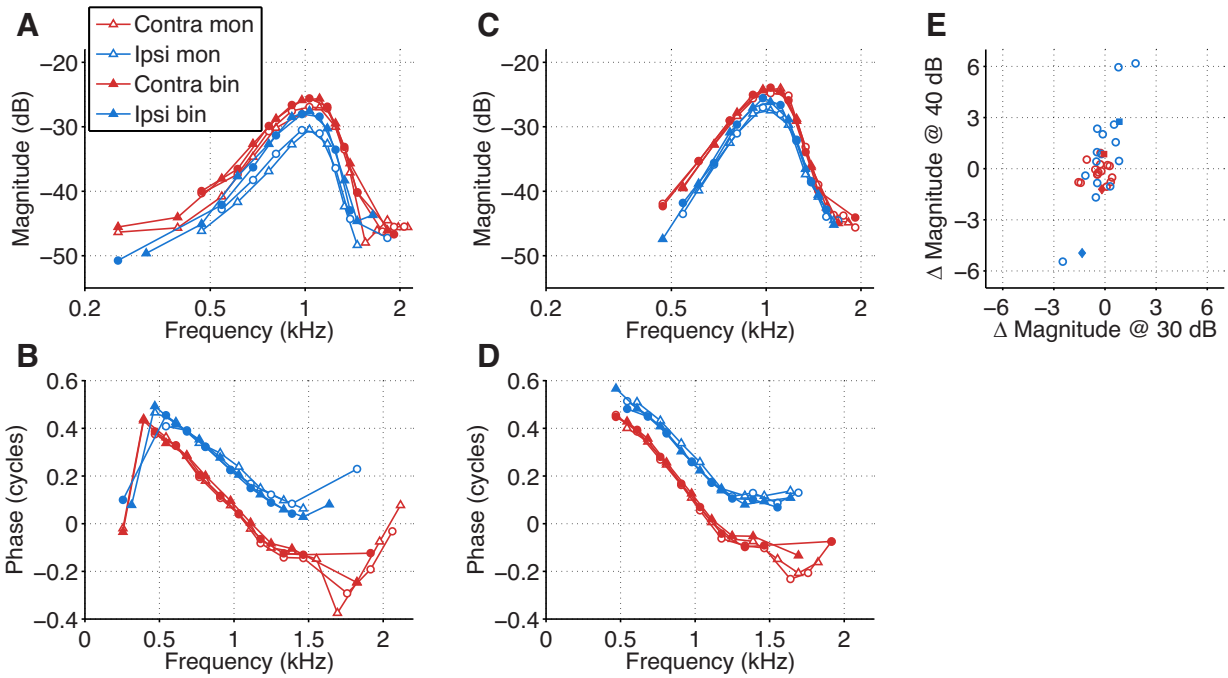

Figure 5. Differences in subthreshold responses to monaural and binaural DZW were reduced at a lower sound intensity. ***A***, Magnitude of responses to monaural and binaural DZW stimuli at 40 dB SPL (cell 81203). At all frequencies, responses to ipsilateral stimulation were clearly smaller for monaural than for binaural stimulation. ***B***, Phase of response to monaural and binaural stimuli at 40 dB SPL for the same cell. Phases were compensated for a delay of 5.0 ms. ***C***, Same as in ***A***, but stimulus intensity was 30 dB SPL. The difference in the responses for the monaural and binaural ipsilateral stimulation condition is strongly reduced. ***D***, Same as in ***B***, but stimulus intensity was 30 dB SPL. ***E***, Comparison of the difference in responses to monaural and binaural stimuli presented at 30 and 40 dB SPL in 17 cells. Differences were smaller for stimuli at 30 dB SPL. Squares represent 81203 used in ***A***-***D***. Diamonds represent cell 89002 (whole-cell recording), which behaved similarly as cells with juxtacellular recordings.

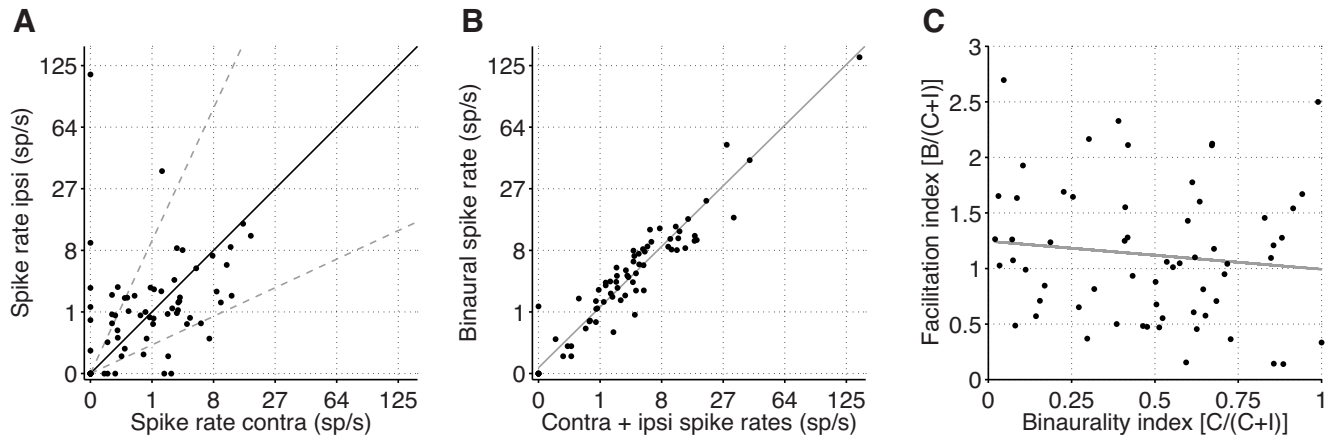

Figure 6. Spike responses to monaural and binaural DZW. ***A***, Comparison of spike rates evoked by monaural ipsilateral and contralateral stimuli plotted on a cubic root scale ($n = 71$). Solid black line indicates the identity line. Dotted lines indicate a 10 times larger spike rate for one ear. ***A***, ***B***, Monaural spike rates were adjusted for spontaneous firing as described in Materials and Methods. ***B***, Comparison of spike rate in response to binaural stimuli and the sum of spike rates in response to ipsilateral and contralateral stimuli ($n = 71$, including 7 cells with very few spikes). Solid line indicates an orthogonal linear regression ($y = 0.99x + 0.15$). ***C***, Comparison of facilitation index (binaural spike rate vs summed monaural spike rates) and binaurality index (contralateral monaural spike rate vs summed monaural spike rates) ($n = 70$ cells). Gray line indicates the regression line ($y = -0.25x + 1.28$; $r = -0.11$; $p = 0.39$). One outlier point with low firing rates and a facilitation index of 8 is not shown and was not taken into account in the fit.

by ipsilateral inputs, but overall, there was no strong bias for either ear. In response to binaurally correlated stimuli, MSO cells generally show binaural facilitation (i.e., the firing rate in response to binaural sound exceeds the sum of the monaurally driven rates) (Goldberg and Brown, 1969; Yin and Chan, 1990; Spitzer and Semple, 1995). This has not been systematically tested for interaurally uncorrelated stimuli, such as the DZW stimulus. We therefore compared the spike rates evoked by the binaural version of the DZW stimulus with the sum of the rates evoked by the ipsilateral and contralateral zwuis stimuli. Evoked spike rates varied greatly between cells, ranging from 0 to 135 spikes/s. Binaural facilitation varied considerably between cells, but there was little evidence for systematic binaural facilitation for the DZW stimuli (Fig. 6*B*). On average, spike rate increased 1.29 ± 0.58-fold ($n = 71$) compared with the predictions obtained by summing the monaural rates; the difference between the two was not significant ($p = 0.53$, Wilcoxon rank sum test); linear regression yielded a line close to the identity line (Fig. 6*B*, solid line), again suggesting that the population of cells did not exhibit binaural facilitation with the DZW stimuli.

The coincidence detection function of the MSO neurons is predicted to be optimal when the size of the ipsilateral and contralateral subthreshold input is matched (Agmon-Snir et al., 1998; Dasika et al., 2007). We therefore tested whether the individual variations in binaural facilitation were correlated with the monaural bias in firing, but this was not the case (Fig. 6*C*).

Beyond merely counting the spikes, we analyzed their timing by assessing the VS and corresponding phase for each of the tone frequencies present in the stimulus. The variation of VS with frequency reflects the frequency tuning of its firing response (van der Heijden and Joris, 2006). As was the case for the subthreshold data (Fig. 2*D*,*E*), the frequency tuning and phase transfer of spikes could be evaluated separately for the two ears, even within a single recording.

Figure 7*A* gives an example of this VS analysis for both the monaurally and binaurally evoked APs. Remarkably, not only during the monaural stimulation, but also for binaural stimulation, the cell showed significant phase-locking to different frequencies. This was not an isolated finding, since, on average, 1.8 of the 2.2 contralateral stimulus components to which the cells showed significant phase-locking during monaural stimulation remained significant during binaural stimulation and the total number of contralateral components with significant phase-locking on average increased to 3.3 of a total of 15 contralateral components during binaural stimulation of the same cell ($n = 71$ cells). For the ipsilateral stimulation, these numbers were 1.7, 2.0, and 3.1, respectively. The frequency tuning of the spikes, as assessed from the VS, was similar to that of the subthreshold data (Fig. 7*B*). The amplitudes of the individual phase-locked subthreshold components were in the μV range in the juxtacellular recordings (Fig. 7*B*), illustrating that these neurons have a remarkable ability to fire on their phase-locked inputs, although for each of them its systematic contribution was only small.

In Figure 7*C*, *D*, the VS in response to binaural DZW is plotted against the VS in response to monaural DZW at the same frequency. This comparison reveals how phase-locking to the stimulus in one ear is affected by presenting independent frequency components to the other ear. This comparison does not consider changes in the associated subthreshold components between binaural and monaural stimulation, but Figure 4 shows that these differences were not systematic. In the illustrated example, there was little decrease in phase-locking during binaural stimulation, although under this condition, many additional frequencies will compete for spike generation at the axon.

If the MSO neuron were an ideal coincidence detector, in the case of a binaural beat stimulus, it would be firing only when the phases from the two ears coincide (i.e., it would be phase-locking at the beat frequency to both ears at the same time). For this hypothetical ideal coincidence detector, stimulating the other ear would not reduce phase-locking to the given ear. The DZW stimulus is a more complex stimulus than the binaural beat, but an ideal coincidence detector in theory would be able to pick out the points in time at which the phases from the many components coincide. This hypothetical cell would thus be able to phase-lock to many components of the DZW stimulus at the same time, finding coincidences to multiple components. However, the data and fits in Figure 7*C*, *D* show that VS was generally reduced during binaural stimulation, indicating that MSO neurons are not ideal coincidence detectors. In Figure 7*C*, *D*, the relationship between S_B, the VS during binaural stimulation, and $S_{C,I}$, the VS during contralateral or ipsilateral stimulation, was

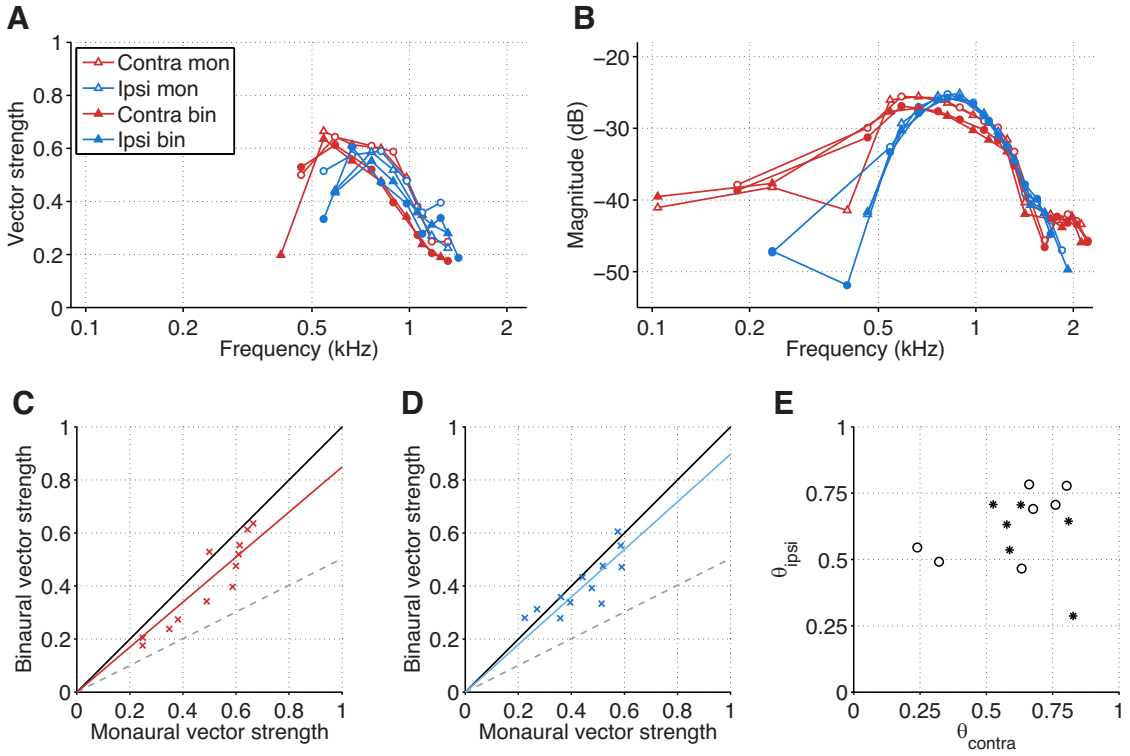

Figure 7. Phase-locking to the individual components of the zwuis stimulus. ***A***, VS versus frequency. Significant ipsilateral (blue) and contralateral (red) components are shown for monaural (open symbols) and binaural (closed symbols) DZW stimulation. ***B***, Magnitude of subthreshold components (compare Fig. 2*D*) obtained from the same recording. ***C***, Crosses ($n = 12$) represent VS to the contralaterally presented components compared between monaural and binaural stimuli. This comparison assesses how phase-locking to the contralateral stimulus is affected by presenting an uncorrelated stimulus to the ipsilateral ear. Unity line (solid black line) is the prediction of a perfect coincidence detector. Dashed line indicates the prediction in case of spike-train superposition (see Materials and Methods). Red line indicates the fit $S_C = \beta_C S_B$, with $\beta_C = 0.85$. θ_C, the normalized β_C, was 0.66. ***D***, Same as in ***C***, but with the ears reversed. Blue line indicates the fit $S_I = \beta_I S_B$ with $\beta_I = 0.90$. θ_I, the normalized β_I, was 0.78. ***E***, Population data of the relation between θ_I and θ_C. Open circles represent cells with good ITD tuning ($n = 7$). *Cells for which recording duration did not permit to test ITD tuning ($n = 6$).

approximately linear. In the cells in which at least three components were significant for both the monaural and the binaural stimulation, we fitted the data to $S_{C,I} = \beta_{C,I} S_B$, where β is the slope of the line fit through the origin (Fig. 7*C*,*D*). On average, β_C was 0.86 ± 0.11 ($n = 29$ cells) and β_I was 0.92 ± 0.18 ($n = 23$ cells). This means that the VS of a component is typically reduced by only ~10% when the other ear is stimulated as well.

To evaluate how much worse the performance of the MSO cells is than the ideal coincidence detector (Fig. 7*C*,*D*, unity line), we next evaluated the opposite case, in which there is no coincidence detection at all. In Figure 7*C*, *D*, the dotted line indicates the prediction for binaural spike-train superposition (see Materials and Methods). The actual data fall between these two extremes. As a metric for where the actual data lie relative to these two extremes, we defined the metric θ (see Materials and Methods). In Figure 7*E*, θ_C and θ_I were plotted against each other for the cells for which both could be assessed. This shows that, in most cells, both were >0.5, suggesting that MSO neurons are good coincidence detectors, which manage to preserve phase-locking to one ear quite adequately when the other ear is stimulated as well, even when this is with incoherent stimuli, as was the case for the DZW stimuli. In a subset of these cells, the recordings were sufficiently stable to allow to test their ITD tuning. Each of these cells showed good ITD tuning (Fig. 7*E*, open circles), even when θ_C or θ_I was ~0.25.

The occasionally large difference in spike rates evoked by ipsilateral or contralateral monaural stimulation (Fig. 6*A*) raises the question what this means for the pivotal function of MSO neurons to detect differences in the arrival times of sounds at both ears. Figure 8*A* shows an extreme example in which significant phase-locking was observed only to the contralateral stimuli. Monaurally excited neurons have been described before within the MSO (e.g., Goldberg and Brown, 1968; Guinan et al., 1972). In this cell, spontaneous rates were 0.3 spikes/s and ipsilateral, contralateral, and binaural rates during DZW stimulation were 0.9, 4.4, and 7.7 spikes/s, respectively. A comparison of subthreshold responses showed only small differences in tuning for ipsilateral and contralateral, with similar BF and only slightly smaller responses to ipsilateral stimuli (Fig. 8*B*). In this cell, we also tested ITD tuning, using noise stimuli presented at different ITDs. The cell showed excellent suprathreshold ITD tuning with a BITD of −0.03 ms and side lobes spaced at intervals predicted by the frequency tuning (Fig. 8*C*). This cell was not an isolated case. In a subpopulation of cells with good ITD tuning, we compared the number of significant VS components for ipsilateral and for contralateral stimulation. Both for the monaural and the binaural case, there was little correlation between the number of ipsilateral and contralateral components. The number of VS components index (C/[C + I]) showed large variability but was not significantly correlated with BITD (Fig. 8*D*). We conclude that asymmetry in the ipsilateral and contralateral impact on spike rates during monaural stimulation is a common phenomenon, and that it is not a good predictor for the ability of an MSO neuron to encode ITDs.

Nonlinear interaction: monodendritic and bidendritic distortion products

The previous analyses have shown that subthreshold inputs sum linearly across the ears (Figs. 2-5), whereas the spike trains reveal

the type of nonlinear interaction ("multiplication") to be expected from a coincidence detector. To test the interaction between each of the components more systematically, we evaluated the degree of linearity of the responses from the inspection of DP2s in the response. The nonlinear interaction among each pair of stimulus components f_m, f_n, may generate sum and difference components at frequencies $f_m + f_n$ and $f_m - f_n$, respectively. By design of the DZW stimulus, both these sum and difference frequencies are unique, and never overlap with primary components (see Materials and Methods). These bilateral inputs involve both dendrites of the MSO cell. Hence, we will call the resulting DP2s bidendritic, although the morphology of the MSO neuron may occasionally deviate from the simple scheme with only two dendrites extending in both directions (Smith, 1995). The MSO is the first place where the two inputs converge, so if they exist, according to the superposition principle these bidendritic DP2s must reflect nonlinear interactions within the MSO cell. Analogously, we will call DP2s whose "parent primaries" were presented to the same ear, monodendritic DP2s. Their origin need not be local to the MSO cell since the parent primaries share the entire monaural pathway projecting to the MSO cell, and second-order nonlinear interaction has been observed in cochlear mechanics (Versteegh and van der Heijden, 2012) and in the auditory nerve in the form of envelope coding (van der Heijden and Joris, 2003). The MSO cell itself could also contribute to monodendritic DP2s (e.g., by dendritic nonlinearities) (Agmon-Snir et al., 1998).

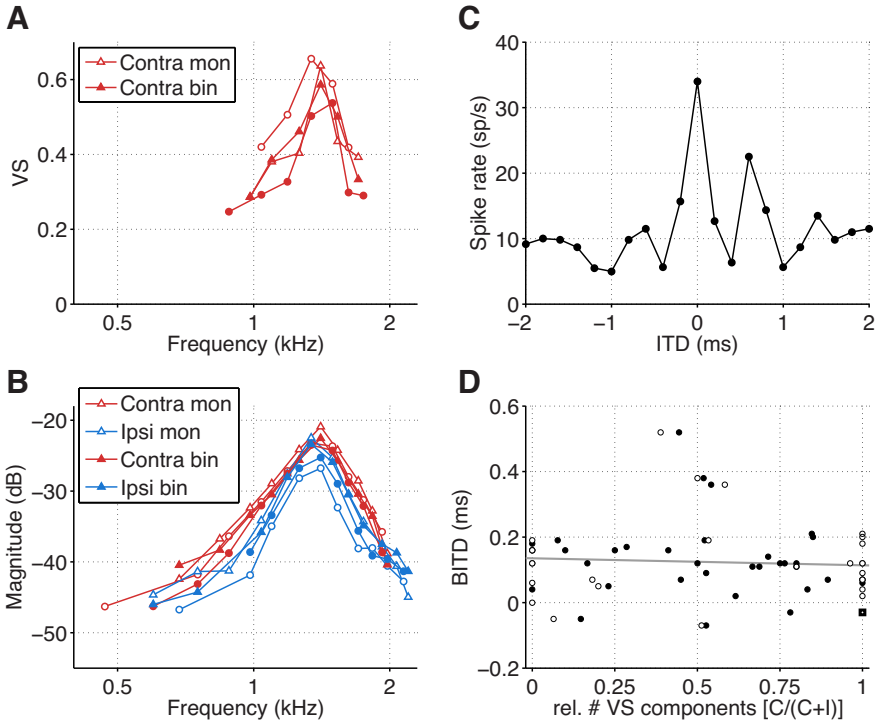

Figure 8. Neurons driven by only one ear can nevertheless have good ITD tuning. ***A***, VS of DZW components of a cell (90004) that phase-locked only to contralateral stimulation. Empty red symbols represent contralateral stimulation. Filled red symbols represent contralateral components during binaural stimulation. ***B***, Subthreshold frequency response. ***C***, ITD tuning curve obtained using noise stimuli presented at different ITDs. ***D***, Binaural disparity between the number of significant VS components was not correlated with the BITD measured in the same cells. Open symbols represent monaural stimulation ($n = 31$ cells). Closed symbols represent binaural DZW stimulation ($n = 33$ cells). Gray line indicates the regression line for the monaural data ($y = -0.02x + 0.135$; $r = -0.07$; $p = 0.69$). Square represents the cell that is illustrated in ***A-C***.

Figure 9*A–C* shows the VS of the spiking response for primaries and DP2s in an example cell during the presentation of monaural or binaural DZW. A large number of both monodendritic (triangles) and bidendritic DP2s (stars) could be observed, which were because of the nonlinear interaction between primaries from the same ear and across the two ears, respectively. For comparison, the subthreshold magnitudes of the primaries are also shown (Fig. 9*D*), which illustrate the good matching between the ipsilateral and contralateral tuning and the relatively small size of primaries outside the region between 0.5 and 1.5 kHz in this cell.

In the cell population, primary components relatively often reached significance as assessed by a Rayleigh test ($p < 0.0001$) compared with the DP2s. In most cases, 53.9% of all primary frequencies within the DZW stimulus, this was for subthreshold only; in 20.9% of all presented primaries, both subthreshold and spiking activity reached significance, and in 0.4% of all primaries only VS was significant. The monodendritic DP2 components were less common, and these numbers across all frequencies were 10.3%, 1.4% and 0.5%, respectively, for subthreshold, subthreshold and AP, and AP only. These distributions were quite different for the bidendritic DP2s, for which the numbers were 0.07%, 0.04% and 0.7%, respectively.

In Figure 10, their relative occurrence is shown as a function of stimulus frequency for primaries (Fig. 10*A*), bidendritic DP2s (Fig. 10*B*), and monodendritic DP2s (Fig. 10*C*). Figure 10*A* illustrates that, between 0.6 and 1.8 kHz, >90% of the primaries reached significance for subthreshold activity alone or with spiking activity, reflecting the ability of the MSO neurons to phase-lock to many different tonal components over a broad frequency range at the same time. Figure 10 also shows the obvious differences between primaries (Fig. 10*A*) and monodendritic DP2s (Fig. 10*C*) on the one hand and bidendritic DP2s (Fig. 10*B*) on the other hand. Whereas most primaries and monodendritic DP2s were subthreshold, the large majority of the bidendritic DP2s were observed only as a significant VS, and only a very small fraction was found in the subthreshold response. The former confirms the nonlinear nature of binaural phase-locking (Fig. 9), and the latter the high degree of linearity in the somatic summation of subthreshold inputs from both dendrites (Figs. 2-5). In contrast, the monodendritic DP2s behave much more like the primaries, with a preponderance of subthreshold-type DP2s (Fig. 10*C*, light brown bars), which might indicate that they are at least already partially present within the inputs to the MSO neurons.

When expressed as a percentage of the number of possible components, significant DP2s appear to be much less frequent than the significant primaries. This is somewhat misleading, since the number of combinations between primaries is much larger than the number of primaries. Moreover, the primary frequencies within the DZW stimulus were chosen to be within the tuning range of most MSO neurons, which means that their sum and difference frequencies often lie outside this range. A better

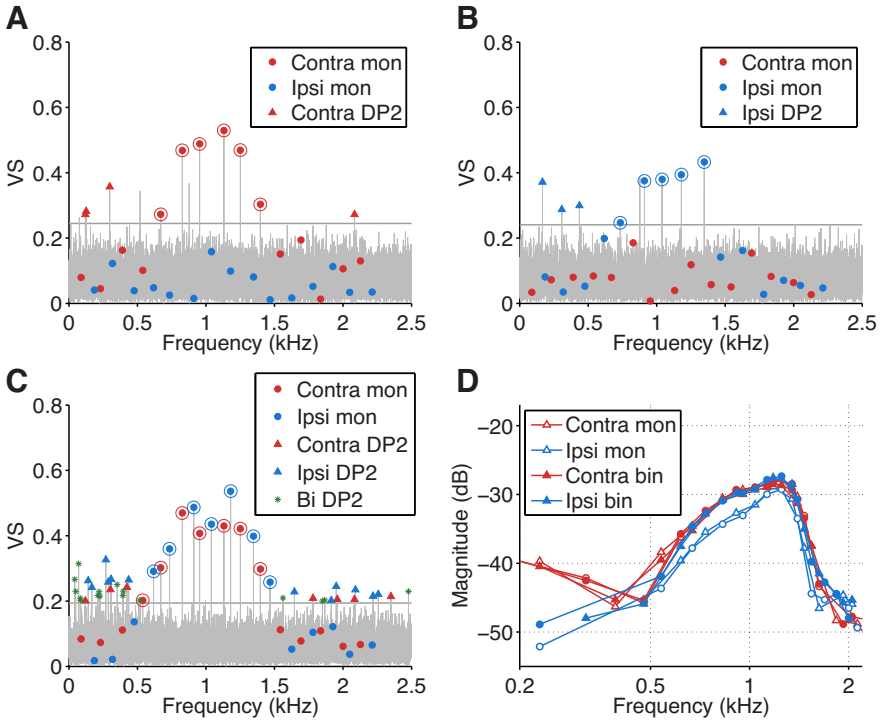

Figure 9. Evidence of nonlinearity in spiking response to DZW stimulus. ***A***, VS of DZW components presented contralaterally (cell 84203). VS was obtained from the Fourier transform of binary spike data. Small filled circles represent the primary components in the auditory stimulus ("Contra mon"). Horizontal gray line indicates the threshold for significance; primaries above this line are shown as a filled circle with a larger circle. Triangles represent the DP2s where both f1 and f2 were in the same ear (i.e., monodendritic DP2s, "Contra DP2"). Only DP2s whose VS was significant have been marked. The response to only one of the two DZW stimulus sets is shown; the other set of frequencies produced similar results. ***B***, Same as in ***A***, but stimulation was ipsilateral. ***C***, Same as in ***A***, but stimulation was binaural. Green asterisks represent the bidendritic DP2s ("Bin DP"), for which f1 and f2 were presented in different ears. ***D***, Magnitude of subthreshold components obtained from the same recording as illustrated in ***A***-***C***.

measure of the relative impact of the DP2s is to calculate their total power, as detailed in Materials and Methods. Their power relative to that of the primaries is shown in Figure 11*A* for subthreshold activity and in Figure 11*B* for VS. On overage, the power of subthreshold DP2 activity was only 4.1 ± 2.3 dB lower than the power of subthreshold primary activity (Fig. 11*A*). The power from subthreshold DP2 activity mostly came from monodendritic DP2s, since the power of subthreshold bidendritic DP2 activity was 29.6 ± 8.6 dB (i.e., ~99.9%) lower than of monodendritic DP2s (Fig. 11*B*). The DP2s also made a substantial contribution to the spiking activity, as the power of suprathreshold DP2 activity was only 2.8 ± 4.5 dB lower than of the suprathreshold primary activity (Fig. 11*C*). For the suprathreshold activity, the bidendritic DP2s contributed much more substantially, as their power was only 4.7 ± 5.2 dB lower than of monodendritic DP2s (Fig. 11*D*). These comparisons thus attest to the ability of MSO neurons to detect coincident inputs. The large contribution of the suprathreshold bidendritic DP2s to the overall power, and their minimal contribution to the subthreshold power, can be readily explained by a linear somatic summation of EPSPs followed by an expansive, nonlinear spike generation mechanism (van der Heijden et al., 2013; Plauška et al., 2016).

Input-output relation

The availability of both subthreshold responses and APs allowed us to analyze the relation between the input and output of the recorded cells. Figure 12*A* shows the relation between the magnitude of a subthreshold input and its corresponding VS for the same primary frequency. Larger subthreshold responses led to higher VSs; and for the range of significant VSs observed in our experiments, this relation was approximately linear. Except for low, marginally significant VSs, the relation could be well captured by a linear fit through the origin. We define the slope of this linear fit (Fig. 12*A*, lines) as the spike-triggering efficacy. It is a measure for the fraction of the total APs that become phase-locked per μV subthreshold component size. In this example, ipsilateral and contralateral primary inputs control the timing of APs with comparable efficacy. The efficacy was generally somewhat lower for the monaural than for the binaural stimulation, but the difference was not large (Fig. 12*B*; 0.92 ± 0.36-fold; $n = 33$). A comparison of VS and DP2s during monaural and binaural stimulation suggests that this reduction is mostly caused by the small reduction in VS for the binaural condition (Fig. 7).

Unexpectedly, we also found several cells showing a large interaural asymmetry in spike-triggering efficacy. An example is shown in Figure 13*A*. The slope for this cell was about twice as large for ipsilateral as for contralateral inputs, both for the monaural as for the binaural stimulus condition. Figure 13*B* summarizes the relative spike triggering efficacies for ipsilateral and contralateral inputs during binaural stimulation, illustrating that, although the efficacy was similar in many cells, in 5 of 33 cells, this ratio differed by >50%. Overall, ipsilateral inputs dominated spike triggering more often than contralateral inputs, in line with the results shown in Figure 6*A*. The asymmetry in spike triggering was observed within the same stimulus period, excluding a change in the recording conditions as a possible explanation.

In Figures 12 and 13, we did not show the input-out relation for monodendritic and bidendritic DP2s. For the bidendritic DP2s, the spike triggering efficacy turned out to be not especially meaningful. As illustrated in Figure 10*B*, the subthreshold bidendritic DP2s are largely absent, indicating that the spikes associated with the bidendritic DP2s are triggered on the linear summation of inputs evoked by primaries from different ears. For the monodendritic DP2s, a much larger fraction was subthreshold type (Fig. 10*C*). Their apparent efficacy, again quantified as the slope of the regression line, was in almost all cells clearly higher than for the primaries. In cells with at least three ipsilateral or contralateral components for both primaries and monodendritic DP2s during binaural DZW stimulation, the slope ratio was 1.77 ± 0.58 ($n = 33$ cells). This suggests that the phase-locking observed at the frequencies associated with these monodendritic DP2s is caused by a mixture of linear and nonlinear components. A component that is already present in the inputs would be expected to have an efficacy that is similar to that of the primaries, whereas a component that would be generated by a reduction of driving force during local dendritic summation (Agmon-Snir et al., 1998; Simon et al., 1999; Dasika et al.,

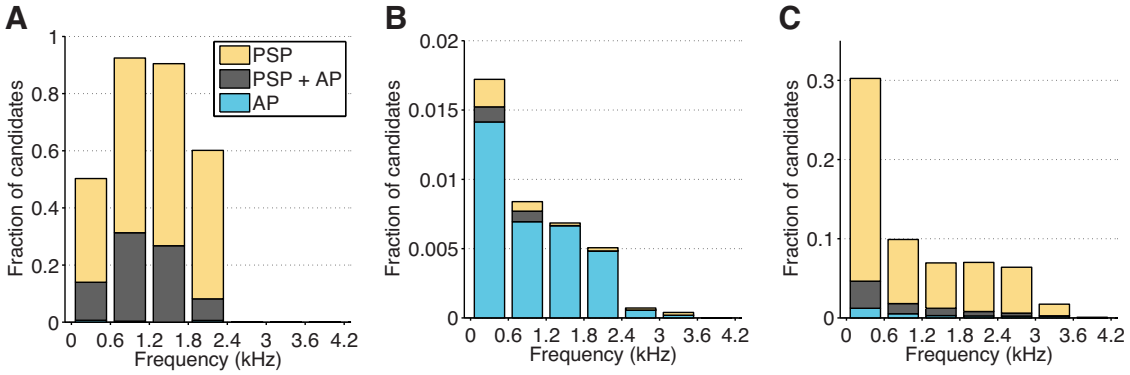

Figure 10. Distribution of significant subthreshold and suprathreshold primary and DP2 components. ***A***, Stacked bar plot represents the distribution of different types of significant primary components as a function of their tone frequencies. The height of the light brown part of the bar indicates the fraction of the total number of primary components in each bracket of frequencies resulting in significant subthreshold activity, but not a significant VS. Blue represents fraction of primary components with only significant VS. Dark brown represents both subthreshold and suprathreshold components significant. Data from 71 cells were pooled. ***B***, Same as in ***A***, but for bidendritic DP2s. ***C***, Same as in ***A***, but for monodendritic DP2s.

2007; Winters et al., 2017; Yamada and Kuba, 2021) would be expected to be associated with a lower efficacy. However, dissecting these different components is difficult without additional knowledge of the inputs to the MSO cells.

The large asymmetries observed in spike triggering efficacy raise the question what the underlying mechanism might be. A difference in input statistics (e.g., concurrent differences in unitary EPSP size and their frequency of occurrence between the dendrites) is a possible candidate. Another possibility is related to the location of the axon. As with almost all neurons, APs are triggered in MSO principal neurons at the axon initial segment (Scott et al., 2007). Anatomical evidence indicates that the axon often does not have a somatic origin in the gerbil MSO (Scott et al., 2005; Rautenberg et al., 2009). A dendritic location would predict that the dendrite on which the axon is located would be favored for spike triggering because of the decrease in amplitudes that the spike from the other dendrite would undergo when passing the soma (Kole and Brette, 2018). In both scenarios, the axonal spike threshold (i.e., the size of the EPSP at the axon initial segment needed to just trigger a spike) should be similar for ipsilateral and contralateral EPSPs, but, as our recordings most likely are predominantly somatic, the prediction for the somatic size of suprathreshold EPSPs is very different for the two scenarios. For the statistical scenario, the suprathreshold EPSPs are expected to be similar for both sides, since evoked spike rates of MSO neurons were generally <100 Hz, suggesting that most spikes are triggered by events that are just suprathreshold. In contrast, for the asymmetric axon localization scenario, it is predicted that a smaller somatic EPSP would be sufficient to trigger a spike from the axon-carrying dendrite than from the other one.

To test which of the two scenarios is more likely, we measured the maximum rate of rise of EPSPs that immediately preceded an AP (Fig. 14*A*), and compared the sizes of these suprathreshold EPSPs during the three stimulus conditions: ipsilateral, contralateral, and binaural DZW stimulation. Figure 14*A* illustrates that the size of the suprathreshold events was in the mV range. This was much larger than the size of the largest phase-locked response in the same juxtacellular recording, which was typically ~50 µV (examples in Figs. 2, 5, 7-9, 12, 13). Figure 14*B* illustrates the inverse relation between EPSPs and EPSP-AP delays, defined here as the delay between the maximum rate of rise of the EPSP that preceded the AP and peak of the AP, showing that larger EPSPs generally trigger APs more rapidly than smaller ones (van der Heijden et al., 2013). A comparison of the three stimulus conditions showed that, in the cell illustrated in Figure 14, suprathreshold EPSPs evoked during contralateral stimulation were on average clearly larger than suprathreshold EPSPs evoked during ipsilateral stimulation (Fig. 14*C*). The size of the suprathreshold EPSPs evoked during binaural stimulation was in between the EPSPs evoked during the two monaural

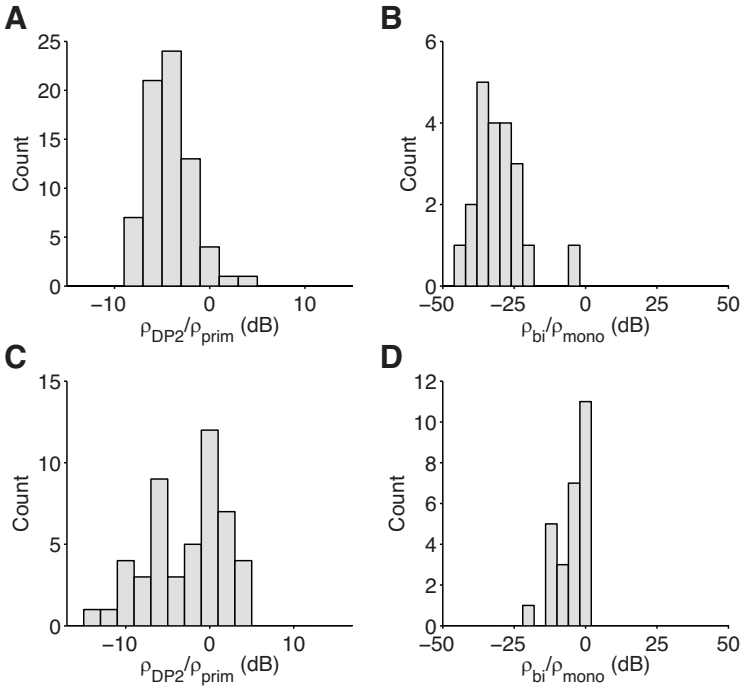

Figure 11. Comparison of the total power of subthreshold and suprathreshold primary and DP2 components evoked by binaural DZW stimulation. ***A***, Power of subthreshold DP2 activity relative to primary activity ($n = 71$ cells). ***B***, Power of subthreshold bidendritic DP2 activity relative to the monodendritic DP2 activity ($n = 21$ cells). ***C***, Power of suprathreshold DP2 activity relative to the primary suprathreshold activity ($n = 49$ cells). ***D***, Power of subthreshold bidendritic DP2 activity relative to the monodendritic DP2 activity ($n = 27$ cells).

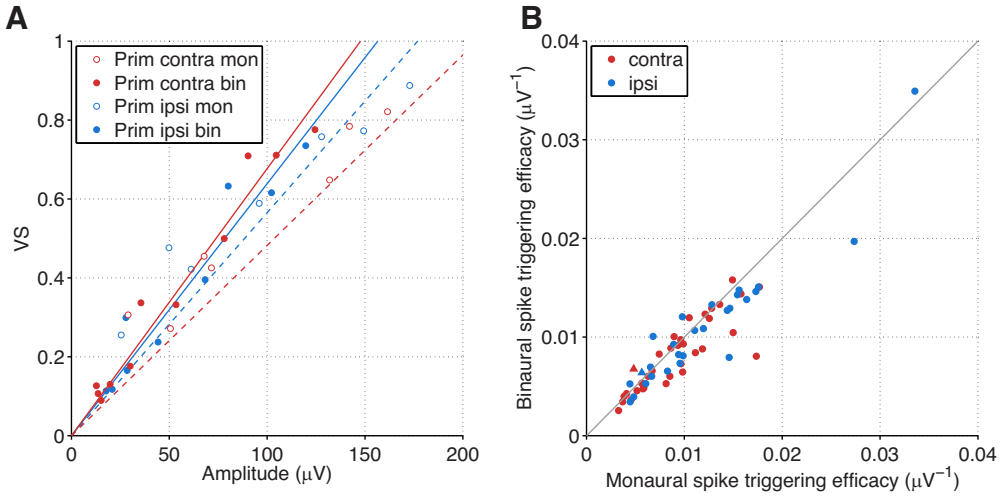

Figure 12. Spike triggering efficacy for monaural and binaural DZW stimulation. ***A***, Relation between VS and the size of the phase-locked response for different frequencies in the DZW stimulus. Only points with both significant VS and significant subthreshold amplitude are shown. Solid lines indicate the regression lines through the origin. In this neuron (92801), spike triggering efficacy was similar for ipsilateral and contralateral inputs. ***B***, Relation between spike triggering efficacy for monaural and binaural ipsilateral ($n = 27$ cells) or contralateral ($n = 35$ cells) stimulation. Triangle represents the cell illustrated in ***A***. Spike triggering efficacy was obtained as in ***A***.

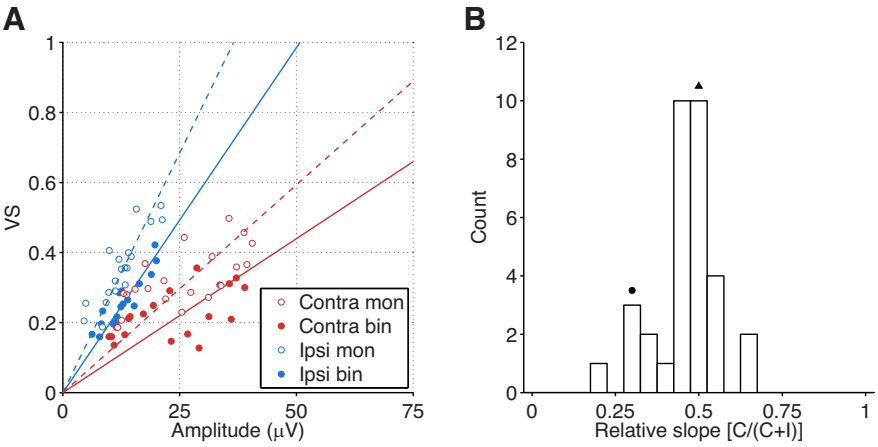

Figure 13. Spike triggering efficacy can be substantially different for ipsilateral and contralateral inputs. ***A***, Relation between VS and the size of the phase-locked response for different frequencies in the DZW stimulus. Solid lines indicate the regression lines through the origin. In this neuron (91307), for both the monaural and binaural stimulus, ipsilateral inputs were associated with higher VSs than contralateral inputs of similar size. ***B***, Histogram represents a comparison of the relative spike triggering efficacy for contralateral and ipsilateral stimuli in a population of cells ($n = 33$). Slopes were obtained as illustrated in ***A***. The relative slope was calculated from the slopes of the ipsilateral and contralateral components during binaural DZW stimulation. Circle and triangle represent the relative slopes obtained for the cell illustrated in ***A*** and in Figure 12*A*, respectively.

conditions, suggesting that they contained EPSPs originating from both dendrites, and indicating that the difference in size between suprathreshold EPSPs evoked by ipsilateral or contralateral stimulation was not caused by a change in recording conditions. In addition, there was little difference in the EPSP-AP delays between the ipsilateral and contralateral monaural stimulus conditions (Fig. 14*D*), suggesting that the somatic difference in average EPSP size does not translate to a size difference at the spike initiation site. A comparison with the spike triggering efficacy in the same cell showed that it was clearly lower for contralateral than for ipsilateral DZW stimulation (Fig. 14*E*, triangle).

A comparison of the relative size of the median suprathreshold EPSP and the relative spike triggering efficacy in the juxtacellular recordings in which this could be calculated showed an inverse correlation, relative inefficient spike triggering was associated with relatively large suprathreshold EPSPs (Fig. 14*E*). The median EPSP-AP delay during ipsilateral and contralateral DZW stimulation correlated well within the same cell ($r = 0.96$), and differed by <40 μs. This small difference was not significantly correlated to the relative spike triggering efficacy (Fig. 14*F*), suggesting that axonal suprathreshold EPSP sizes were similar, even when somatic EPSP sizes differed considerably. In conclusion, the observed inverse correlation between the relative size of the median suprathreshold EPSP and the relative spike triggering efficacy agrees with the scenario in which differences in spike triggering efficacy are caused by the location of the axon on the dendrite with the higher efficacy.

Discussion

We studied the response of MSO neurons to a new multitone stimulus, which we named DZW. The DZW stimulus is a generalization of the binaural beat stimulus; its design allowed the unambiguous identification not only of each primary, but also of each 2DP. The good phase-locking abilities of the MSO neurons resulted in a rich dataset, allowing many different comparisons between subthreshold and suprathreshold events, monaural and binaural responses, and tone response interactions within and between dendrites. Their concurrent presence in the same dataset allowed a much more reliable comparison of their relative sizes. These comparisons led to the following main observations and conclusions. We found evidence for linear somatic summation of dendritic inputs, as inputs from one ear depended little on the presence or absence of sound-evoked inputs at the other ear and subthreshold bidendritic DP2s were rare. We found ample evidence that MSO neurons are excellent coincidence detectors: phase-locking to stimulus tones decreased only little for binaural stimuli, suprathreshold bidendritic DP2s were common, and a subset of neurons with highly asymmetric inputs

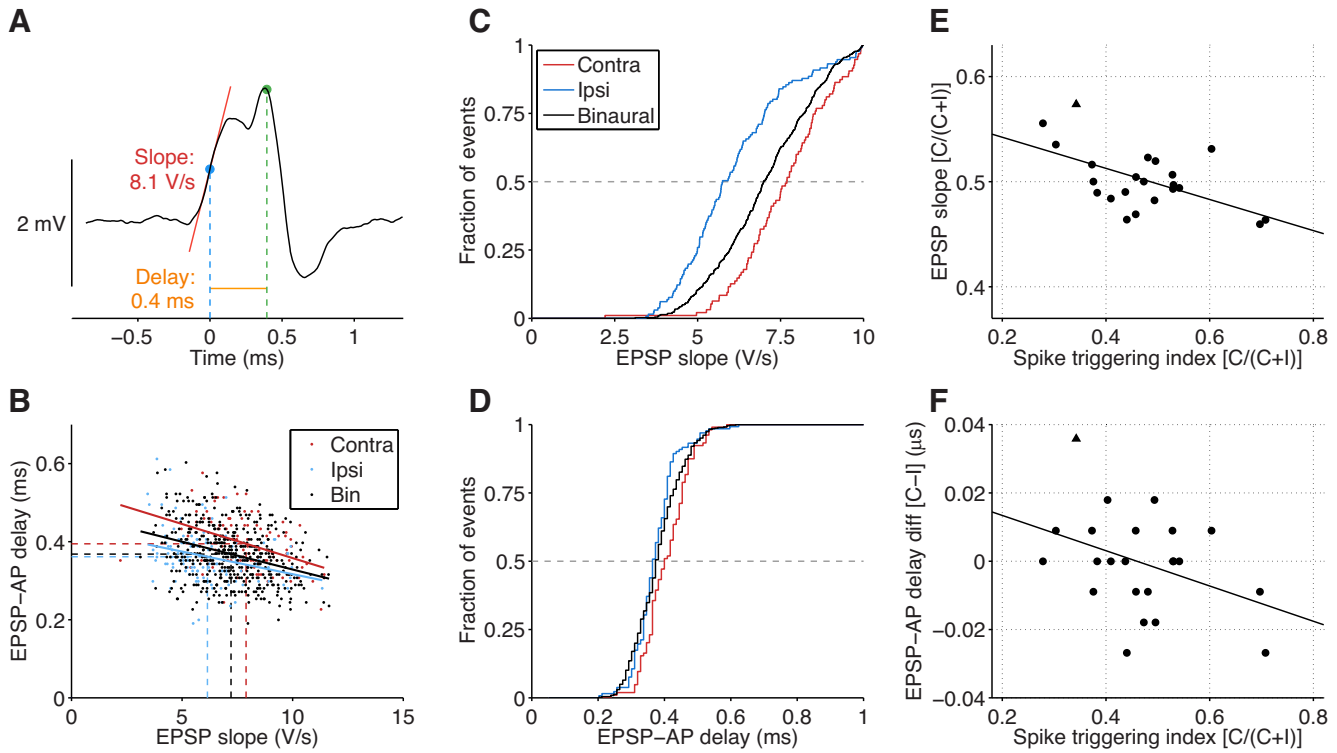

Figure 14. Lower spike triggering efficacy is associated with larger suprathreshold EPSPs. ***A***, Measurement of maximum rate of rise of suprathreshold EPSP and EPSP-AP delay. ***B***, Scatterplot represents the relation between EPSP-AP delay and the maximum rate of rise of suprathreshold EPSPs during ipsilateral monaural stimulation (blue; $n = 132$), contralateral monaural stimulation (red; $n = 104$), or binaural DZW stimulation (black; $n = 466$) for the same cell as in ***A***. Broken lines indicate median values. Solid lines indicate regression lines showing that larger EPSPs trigger APs more rapidly. ***C***, Cumulative plots of suprathreshold EPSPs for the same data as shown in ***B***. ***D***, Cumulative plots of EPSP-AP delays for the same data as shown in ***B***. The horizontal line intersects with the median delay. ***E***, Relation between the relative size of the median EPSP slope and the relative size of the spike triggering efficacy. Solid line indicates the regression line ($y = -0.15x + 0.57$; $r = -0.56$; $p = 0.007$; $n = 23$). Triangle represents the cell illustrated in ***A-D***. ***F***, Relation between the difference in the median EPSP-AP delay during contralateral and ipsilateral monaural DZW stimulation and the relative size of the spike triggering efficacy. Solid line indicates the regression line ($y = -0.05x + 0.02$; $r = -0.38$; $p = 0.072$; $n = 23$). Triangle represents the cell illustrated in ***A-D***.

nevertheless showed good ITD sensitivity. Finally, in some neurons, spike triggering efficacy differed substantially for inputs from both ears, suggesting a dendritic axonal origin.

Linear somatic summation of synaptic inputs

Closed-field stimulation allowed a much higher interaural level difference than gerbils normally experience (Maki and Furukawa, 2005). DZW is thus a fully incoherent stimulus with nonphysiologically high interaural level differences. Using the DZW stimulus, we found in both juxtacellular and whole-cell recordings that, in most cells, the amplitudes of the subthreshold events of one ear were hardly affected by the addition of (incoherent) stimuli to the other ear. In some neurons, there were small effects, often close to the best frequency. However, these effects largely disappeared at a lower sound intensity (Fig. 5), suggesting that they may have been because of acoustic crosstalk between the ears, to which MSO neurons as coincidence detectors obviously are quite sensitive. Additional evidence for crosstalk effects is that the threshold for ipsilateral stimulation of the MNTB principal neurons, which does not have direct ipsilateral sound inputs (Thompson and Schofield, 2000), was also observed at ~40 dB higher than the contralateral threshold (Y.M., unpublished results). This suggests that dendritic inputs from both ears sum linearly, in good agreement with our earlier results using binaural beats (van der Heijden et al., 2013) and with the paucity of significant bidendritic subthreshold DP2s. Apparently, the relatively small size of synaptic somatic events results in only limited reduction in their driving force (Agmon-Snir et al., 1998; Simon et al., 1999; Grau-Serrat et al., 2003; Dasika et al., 2007). Similarly, voltage-dependent conductance changes are apparently either small, or conspire to linearize responses (Svirskis et al., 2004; Mathews et al., 2010; Scott et al., 2010; Khurana et al., 2011; Remme and Rinzel, 2011; Huguet et al., 2017). In contrast, Franken et al. (2015) observed that ITD tuning measured with binaural beats deviated from instantaneous cross-correlation predictions using subthreshold responses, indicative of nonlinear interactions between voltage-dependent and synaptic conductances. We previously found that the relationship between firing rate and ITD could be well predicted from subthreshold monaural responses (Plauška et al., 2016). In Franken et al. (2015), stimuli were generally presented at high intensities, and at frequencies far from the best frequency, whereas we used wideband stimuli not far above hearing threshold, hampering a direct comparison.

Our results also indicate that the contribution of shunting-type synaptic inhibition has to be relatively small. MSO neurons receive somatic inhibitory inputs from both the ipsilateral MNTB and the contralateral lateral nucleus of the trapezoid body (Thompson and Schofield, 2000). Adding sound stimuli to the other ear will therefore recruit not only dendritic excitatory inputs, but also somatic inhibition, predicting reduced EPSP sizes of the first ear (Silver, 2010), which is not what we observed. However, these conclusions are only indirect, and pharmacological studies would be needed to more conclusively delineate the role of synaptic inhibition within the MSO (Grothe and Sanes,

1994; Brand et al., 2002; Pecka et al., 2008; Roberts et al., 2013; Myoga et al., 2014; Franken et al., 2015).

MSO neurons are efficient coincidence detectors

In the DZW stimulus, each tone frequency is unique and its VS thus provides an estimate for its relative contribution to the MSO output. Interestingly, the MSO neurons showed a significant VS to many different components within the stimulus, both to primaries and to tone combinations. This was remarkable since the average amplitude for subthreshold components, as estimated by Fourier analysis, was quite small, in the μV range even for whole-cell recordings. However, within a given cell, its size predicted VS well (Fig. 12).

VSs decreased little during binaural stimulation, in agreement with results obtained in the rabbit MSO, where responses to tones and binaural beats were compared (Batra et al., 1997). This agrees with the lack of a decrease in the size of subthreshold primaries, but it is nevertheless remarkable since in the binaural version of the DZW stimulus the cell will also start to phase-lock to the stimuli presented to the other ear. MSO cells apparently efficiently use the incidental coincidences offered by these rich stimuli, as also borne out by the prominent emergence of bidendritic DP2s in the binaural DZW version.

We observed a remarkably large variability in the relative impact of inputs from both ears. Both the relative size of the largest subthreshold primary component for the two ears (e.g., Figs. 2*E*, 3*D*) and the number of significant VS components (Fig. 8) differed considerably between cells. This was somewhat unexpected, as coincidence detection is predicted to be optimal when the inputs from both ears are matched in size (Agmon-Snir et al., 1998; Dasika et al., 2007). Similar results were obtained in the rabbit MSO, where the VS for monaural ipsilateral and contralateral tone stimuli showed, if anything, an inverse correlation (Batra et al., 1997). However, unexpectedly, even in neurons with large asymmetries both in subthreshold component size and in monaural VS, good ITD tuning could often still be observed (Fig. 8). The combination of linear somatic summation and nonlinear spike generation apparently allows MSO neurons to robustly perform their core function, coincidence detection, even with asymmetrically sized inputs originating from both ears.

Is there a binaural advantage?

The DZW stimulus produced some results that appeared, at first sight, at odds with the role of the MSO as a coincidence detector. For example, overall, the MSO neurons showed little or no binaural facilitation for DZW. Possibly, during monaural stimulation, the MSO neurons are helped by the presence of spontaneous events at the other ear for "accidental" coincidences (Colburn et al., 1990; van der Heijden et al., 2013), whereas during binaural stimulation they also have to rely on accidental coincidences offered by the incoherent stimuli of the other ear. This suggests that DZW may not be the best stimulus to study the binaural advantage. As a wideband extension of the binaural beat stimulus, the somatic fluctuations triggered by any of the many tones are more limited, which would tend to linearize the spike generation mechanism. On the other hand, the ability to uniquely identify the DP2s as either monodendritic or bidendritic potentially makes it feasible to compare how efficiently both of them trigger spikes. The relative spike triggering efficacy of intradendritic and interdendritic coincidences has been predicted to differ substantially (Agmon-Snir et al., 1998; Dasika et al., 2007; Franken et al., 2014). However, a test of this prediction turned out to be difficult. Whereas subthreshold bidendritic DP2s were observed only very infrequently, in agreement with the linear somatic summation of inputs, monodendritic subthreshold DP2s were quite common. The latter could be generated within a dendrite or already be present in the inputs. Intradendritic generation is a feasible scenario, since synaptic potentials are much larger in the dendrite than in the soma of MSO neurons (Winters et al., 2017). Sublinear integration because of reduced driving force can therefore be expected to be prominent in a compact dendrite with large synaptic potentials, such as the MSO neuron (Agmon-Snir et al., 1998; Dasika et al., 2007; Silver, 2010; Tran-Van-Minh et al., 2015; Winters et al., 2017). However, there is also good evidence for nonlinear interactions between tones at different stages peripheral from the MSO, including the cochlea (Cooper et al., 2018). Our present results unfortunately do not allow disentangling the relative contribution of these two sources. Nevertheless, the paucity of bidendritic subthreshold DP2s and the prominence of bidendritic suprathreshold DP2s attested to the ability of the MSO neurons to find "accidental" coincidences within the incoherent sea offered by the DZW stimulus. This conclusion is further supported by the substantial total power of the suprathreshold bidendritic DP2s, which approached that of the primaries (Fig. 11), and by the ability of MSO neurons to phase-lock to many different components within the bidendritic DZW (Fig. 7).

Differential spike triggering efficacy of ipsilateral and contralateral inputs

In a minority of cells, we observed that the spike triggering efficacy for ipsilateral and contralateral inputs differed considerably. This observation was unexpected and we considered several possible origins. First, the nonlinear relationship between EPSP size and probability of initiating an AP (van der Heijden et al., 2013) predicts that an infrequent, large input will have a larger efficacy than a frequent, small input (e.g., low release probability with large quantal size vs high release probability with low quantal size). Second, the spike triggering efficacy might be lower because the axon originated from the other dendrite. A dendritic origin would have important consequences for axonal signaling within the MSO (Zhou et al., 2005; Goldwyn et al., 2019). This scenario would predict that the individual suprathreshold EPSPs from the side with the lower efficacy will have to be larger to compensate for their somatic attenuation (Kole and Brette, 2018). This was indeed observed (Fig. 14). Although for definitive proof histologic confirmation would be needed, the fraction of neurons with asymmetrical spike triggering efficacies matched earlier histologic observations in the gerbil. Remarkably, whereas a dendritic origin is uncommon in the gerbil MSO (Scott et al., 2005; Rautenberg et al., 2009), it is much more common in cats or guinea pigs (Kiss and Majorossy, 1983; Smith, 1995). It is not obvious what the advantage of a dendritic origin might be for MSO neurons. In the guinea pig, axons typically originate on the lateral side, so a role in compensating for the longer internal delay of contralateral inputs seems unlikely. A recent modeling study argued that strong soma-to-axon coupling has advantages for both coincidence detection and efficient spike generation (Goldwyn et al., 2019). The core business of MSO neurons, coincidence detection, is optimal when the inputs from both ears are matched. The axon-carrying dendrite will be heavily favored for AP initiation (Kole and Brette, 2018), and this effect can be expected to be further enhanced during somatic inhibition. One would therefore expect a compensating mechanism in these

neurons to allow the impacts of both ears to become more matched again. Our dataset was too small to test this, although we anecdotally observed good ITD tuning in the presence of strong asymmetries in spike triggering efficacy. This puzzling observation warrants a follow-up study of the relationship between the structure and function of MSO principal neurons, which would hopefully result in a better understanding of the possible significance of a dendritic axonal origin.

References

Agmon-Snir H, Carr CE, Rinzel J (1998) The role of dendrites in auditory coincidence detection. Nature 393:268–272.

Batra R, Kuwada S, Fitzpatrick DC (1997) Sensitivity to interaural temporal disparities of low- and high-frequency neurons in the superior olivary complex: II. Coincidence detection. J Neurophysiol 78:1237–1247.

Biedenbach MA, Freeman WJ (1964) Click-evoked potential map from the superior olivary nucleus. Am J Physiol 206:1408–1414.

Brand A, Behrend O, Marquardt T, McAlpine D, Grothe B (2002) Precise inhibition is essential for microsecond interaural time difference coding. Nature 417:543–547.

Clark GM, Dunlop CW (1968) Field potentials in the cat medial superior olivary nucleus. Exp Neurol 20:31–42.

Colburn HS, Han YA, Culotta CP (1990) Coincidence model of MSO responses. Hear Res 49:335–346.

Cooper NP, Vavakou A, van der Heijden M (2018) Vibration hotspots reveal longitudinal funneling of sound-evoked motion in the mammalian cochlea. Nat Commun 9:3054.

Dasika VK, White JA, Colburn HS (2007) Simple models show the general advantages of dendrites in coincidence detection. J Neurophysiol 97:3449–3459.

Franken TP, Bremen P, Joris PX (2014) Coincidence detection in the medial superior olive: mechanistic implications of an analysis of input spiking patterns. Front Neural Circuits 8:42.

Franken TP, Roberts MT, Wei L, Golding NL, Joris PX (2015) In vivo coincidence detection in mammalian sound localization generates phase delays. Nat Neurosci 18:444–452.

Galambos R, Schwartzkopff J, Rupert A (1959) Microelectrode study of superior olivary nuclei. Am J Physiol 197:527–536.

Goldberg JM, Brown PB (1968) Functional organization of the dog superior olivary complex: an anatomical and electrophysiological study. J Neurophysiol 31:639–656.

Goldberg JM, Brown PB (1969) Response of binaural neurons of dog superior olivary complex to dichotic tonal stimuli: some physiological mechanisms of sound localization. J Neurophysiol 32:613–636.

Goldwyn JH, McLaughlin M, Verschooten E, Joris PX, Rinzel J (2017) Signatures of somatic inhibition and dendritic excitation in auditory brainstem field potentials. J Neurosci 37:10451–10467.

Goldwyn JH, Remme MW, Rinzel J (2019) Soma-axon coupling configurations that enhance neuronal coincidence detection. PLoS Comput Biol 15:e1006476.

Grau-Serrat V, Carr CE, Simon JZ (2003) Modeling coincidence detection in nucleus laminaris. Biol Cybern 89:388–396.

Grothe B, Sanes DH (1994) Synaptic inhibition influences the temporal coding properties of medial superior olivary neurons: an in vitro study. J Neurosci 14:1701–1709.

Guinan JJ Jr, Norris BE, Guinan SS (1972) Single auditory units in the superior olive complex II: tonotopic organization and locations of unit categories. Int J Neurosci 4:147–166.

Huguet G, Meng X, Rinzel J (2017) Phasic firing and coincidence detection by subthreshold negative feedback: divisive or subtractive or, better, both. Front Comput Neurosci 11:3.

Johnson DH (1974) The response of single auditory-nerve fibers in the cat to single tones: synchrony and average discharge rate. Cambridge, MA: Massachusetts Institute of Technology.

Khurana S, Remme MW, Rinzel J, Golding NL (2011) Dynamic interaction of I_h and $I_{K\text{-}LVA}$ during trains of synaptic potentials in principal neurons of the medial superior olive. J Neurosci 31:8936–8947.

Kiss A, Majorossy K (1983) Neuron morphology and synaptic architecture in the medial superior olivary nucleus: light- and electron microscope studies in the cat. Exp Brain Res 52:315–327.

Kole MH, Brette R (2018) The electrical significance of axon location diversity. Curr Opin Neurobiol 51:52–59.

Kuokkanen PT, Ashida G, Carr CE, Wagner H, Kempter R (2013) Linear summation in the barn owl's brainstem underlies responses to interaural time differences. J Neurophysiol 110:117–130.

Kuwabara N, Zook JM (1999) Local collateral projections from the medial superior olive to the superior paraolivary nucleus in the gerbil. Brain Res 846:59–71.

Langford TL (1984) Responses elicited from medial superior olivary neurons by stimuli associated with binaural masking and unmasking. Hear Res 15:39–50.

Lu Y, Liu Y, Curry RJ (2018) Activity-dependent synaptic integration and modulation of bilateral excitatory inputs in an auditory coincidence detection circuit. J Physiol 596:1981–1997.

Maier JK, Klump GM (2006) Resolution in azimuth sound localization in the Mongolian gerbil (*Meriones unguiculatus*). J Acoust Soc Am 119:1029–1036.

Maki K, Furukawa S (2005) Acoustical cues for sound localization by the Mongolian gerbil, *Meriones unguiculatus*. J Acoust Soc Am 118:872–886.

Mathews PJ, Jercog PE, Rinzel J, Scott LL, Golding NL (2010) Control of submillisecond synaptic timing in binaural coincidence detectors by K_v1 channels. Nat Neurosci 13:601–609.

McLaughlin M, Verschooten E, Joris PX (2010) Oscillatory dipoles as a source of phase shifts in field potentials in the mammalian auditory brainstem. J Neurosci 30:13472–13487.

Meenderink SW, van der Heijden M (2011) Distortion product otoacoustic emissions evoked by tone complexes. J Assoc Res Otolaryngol 12:29–44.

Moushegian G, Rupert AL, Gidda JS (1975) Functional characteristics of superior olivary neurons to binaural stimuli. J Neurophysiol 38:1037–1048.

Myoga MH, Lehnert S, Leibold C, Felmy F, Grothe B (2014) Glycinergic inhibition tunes coincidence detection in the auditory brainstem. Nat Commun 5:3790.

Pecka M, Brand A, Behrend O, Grothe B (2008) Interaural time difference processing in the mammalian medial superior olive: the role of glycinergic inhibition. J Neurosci 28:6914–6925.

Plauška A, Borst JG, van der Heijden M (2016) Predicting binaural responses from monaural responses in the gerbil medial superior olive. J Neurophysiol 115:2950–2963.

Plauška A, van der Heijden M, Borst JG (2017) A test of the stereausis hypothesis for sound localization in mammals. J Neurosci 37:7278–7289.

Rautenberg PL, Grothe B, Felmy F (2009) Quantification of the three-dimensional morphology of coincidence detector neurons in the medial superior olive of gerbils during late postnatal development. J Comp Neurol 517:385–396.

Ravicz ME, Rosowski JJ, Voigt HF (1992) Sound-power collection by the auditory periphery of the Mongolian gerbil *Meriones unguiculatus*. I: Middle-ear input impedance. J Acoust Soc Am 92:157–177.

Remme MW, Rinzel J (2011) Role of active dendritic conductances in subthreshold input integration. J Comput Neurosci 31:13–30.

Roberts MT, Seeman SC, Golding NL (2013) A mechanistic understanding of the role of feedforward inhibition in the mammalian sound localization circuitry. Neuron 78:923–935.

Ryan A (1976) Hearing sensitivity of the mongolian gerbil, *Meriones unguiculatis*. J Acoust Soc Am 59:1222–1226.

Scott LL, Mathews PJ, Golding NL (2005) Posthearing developmental refinement of temporal processing in principal neurons of the medial superior olive. J Neurosci 25:7887–7895.

Scott LL, Hage TA, Golding NL (2007) Weak action potential backpropagation is associated with high-frequency axonal firing capability in principal neurons of the gerbil medial superior olive. J Physiol 583:647–661.

Scott LL, Mathews PJ, Golding NL (2010) Perisomatic voltage-gated sodium channels actively maintain linear synaptic integration in principal neurons of the medial superior olive. J Neurosci 30:2039–2050.

Silver RA (2010) Neuronal arithmetic. Nat Rev Neurosci 11:474–489.

Simon JZ, Carr CE, Shamma SA (1999) A dendritic model of coincidence detection in the avian brainstem. Neurocomputing 26:263–269.

Smith PH (1995) Structural and functional differences distinguish principal from nonprincipal cells in the guinea pig MSO slice. J Neurophysiol 73:1653–1667.

Spitzer MW, Semple MN (1995) Neurons sensitive to interaural phase disparity in gerbil superior olive: diverse monaural and temporal response properties. J Neurophysiol 73:1668–1690.

Svirskis G, Kotak V, Sanes DH, Rinzel J (2004) Sodium along with low-threshold potassium currents enhance coincidence detection of subthreshold noisy signals in MSO neurons. J Neurophysiol 91:2465–2473.

Thompson AM, Schofield BR (2000) Afferent projections of the superior olivary complex. Microsc Res Tech 51:330–354.

Tran-Van-Minh A, Cazé RD, Abrahamsson T, Cathala L, Gutkin BS, DiGregorio DA (2015) Contribution of sublinear and supralinear dendritic integration to neuronal computations. Front Cell Neurosci 9:67.

van der Heijden M, Joris PX (2003) Cochlear phase and amplitude retrieved from the auditory nerve at arbitrary frequencies. J Neurosci 23:9194–9198.

van der Heijden M, Joris PX (2006) Panoramic measurements of the apex of the cochlea. J Neurosci 26:11462–11473.

van der Heijden M, Lorteije JA, Plauška A, Roberts MT, Golding NL, Borst JG (2013) Directional hearing by linear summation of binaural inputs at the medial superior olive. Neuron 78:936–948.

Versteegh CP, van der Heijden M (2012) Basilar membrane responses to tones and tone complexes: nonlinear effects of stimulus intensity. J Assoc Res Otolaryngol 13:785–798.

Winters BD, Jin SX, Ledford KR, Golding NL (2017) Amplitude normalization of dendritic EPSPs at the soma of binaural coincidence detector neurons of the medial superior olive. J Neurosci 37:3138–3149.

Yamada R, Kuba H (2021) Dendritic synapse geometry optimizes binaural computation in a sound localization circuit. Sci Adv 7:eabh0024.

Yin TC, Chan JC (1990) Interaural time sensitivity in medial superior olive of cat. J Neurophysiol 64:465–488.

Zhou Y, Carney LH, Colburn HS (2005) A model for interaural time difference sensitivity in the medial superior olive: interaction of excitatory and inhibitory synaptic inputs, channel dynamics, and cellular morphology. J Neurosci 25:3046–3058.